Structural and molecular bases to IRE1 activity modulation

Timothy Langlais, Diana Pelizzari-Raymundo, Sayyed Jalil Mahdizadeh, Nicolas Gouault, François Carreaux, Eric Chevet, Leif A. Eriksson, Xavier Guillory

Structural and molecular bases to IRE1 activity modulation

Langlais T.[1], Pelizzari-Raymundo D.[2,3], Mahdizadeh S. J.[4], Gouault N.[1], Carreaux F.[1], Chevet E.[2,3], Eriksson L. A.[4], Guillory X.[1,2,3]

[1]Univ Rennes, CNRS, ISCR (Institut des Sciences Chimiques de Rennes) UMR 6226, Rennes 35042. [2]Proteostasis & Cancer Team INSERM U1242 « Chemistry, Oncogenesis Stress Signaling », Université de Rennes, Rennes, France. [3]Centre de Lutte contre le Cancer Eugène Marquis, Rennes, France. [4]Department of Chemistry and Molecular Biology, University of Gothenburg, Göteborg, Sweden.

Keywords: ER Stress • Unfolded Protein Response • IRE1 • Structure-Based Drug Design (SBDD) • Structure Activity Relationship (SAR)

Correspondence to XG: xavier.guillory@univ-rennes1.fr

Abstract

The Unfolded Protein response is an adaptive pathway triggered upon alteration of endoplasmic reticulum (ER) homeostasis. It is transduced by three major ER stress sensors, among which the Inositol Requiring Enzyme 1 (IRE1) is the most evolutionary conserved. IRE1 is an ER-resident type I transmembrane protein exhibiting an ER luminal domain that senses the protein folding status and a catalytic kinase and RNase cytosolic domain. In recent years, IRE1 has emerged as a relevant therapeutic target in various diseases including degenerative, inflammatory and metabolic pathologies and cancer. As such several drugs altering IRE1 activity were developed that target either catalytic activity and showed some efficacy in preclinical pathological mouse models. In this review, we describe the different drugs identified to target IRE1 activity as well as their mode of action from a structural perspective, thereby identifying common and different modes of action. Based on this information we discuss on how new IRE1-targeting drugs could be developed that outperform the currently available molecules.

Introduction

The endoplasmic reticulum (ER) is the first membranous compartment of the secretory pathway in eukaryotes. It is a calcium store with concentrations 1000 to 10000 times higher than in the cytosol and maintains lipid homeostasis [1]. The ER is also the gateway to the secretory pathway and is instrumental for the proper folding of secretory and transmembrane proteins [1]. As such, it represents a critical machinery through which proteins destined to exert their functions in other cellular compartments must traffic to acquire their correct conformation and post-translational modifications. It has previously been demonstrated that the ER and its functionality is important for the composition of the Golgi complex, the plasma membrane, lipid droplets or the phagosome (autophagosome and lysosomes) [2,3]. Moreover, this compartment is in tight contact with mitochondria, through the mitochondrial-associated membranes (MAMs) or with endosomes or lysosomes [4,5].

When the balance between the cellular protein folding demand and the ER capacity is disrupted, improperly folded secretory and transmembrane proteins accumulate in the ER, a situation known as ER stress [6]. To cope with stress, the ER triggers an adaptive response named the Unfolded Protein Response (UPR). The UPR is transduced by three main ER resident sensors named Inositol Requiring Enzyme 1 alpha (IRE1α, hereafter referred to as IRE1), Protein Kinase RNA-like ER Kinase (PERK) and Activating Transcription Factor 6 (ATF6). Activation of the UPR sensors has as principal purpose to alleviate the stress and is known as the adaptive UPR. If the stress cannot be resolved, the UPR instead triggers apoptosis, referred to as terminal UPR. However, the mechanisms allowing the switch between adaptive and terminal UPR remain ill-characterized. Among the possible candidates, the IRE1 pathway being greatly conserved through evolution plays crucial roles in both physiological and pathological ER stress. Mammals express two IRE1 paralogues: IRE1α and IRE1β. IRE1α (named hereafter as IRE1) is ubiquitously expressed and contributes to XBP1 mRNA splicing. IRE1β expression is predominant in intestinal and lung epithelia, and deletion of IRE1β in mice increases their sensitivity to experimental colitis induced by dextran sodium sulfate [7]. Recently, it was demonstrated that IRE1β might negatively regulate IRE1α signaling in response to endoplasmic reticulum stress [8]. IRE1 is an ER transmembrane protein activated after binding immunoglobulin protein (BiP) dissociation and/or direct binding

of improperly folded proteins [9,10]. IRE1 is characterized by the presence of both kinase and endoribonuclease domains in its cytosolic region. After its dimerization/oligomerization, IRE1 trans-autophosphorylates allowing the recruitment of TNF receptor-associated factor 2 (TRAF2) and the subsequent activation of the c-Jun N-terminal kinase (JNK) pathway [1]. IRE1 phosphorylation also yields a conformational change which activates the RNase domain and leads to unconventional splicing of the *XBP1* mRNA and the expression of a major UPR transcription factor XBP1s [1,6]. Importantly, the ligation following the IRE1-mediated excision of the 26nt intron in the *XBP1* mRNA is catalyzed by the tRNA ligase RtcB in mammals [11–13]. Through its RNase domain, IRE1 also accounts for the cleavage of mRNA, rRNA and miRNA sequences, a process named Regulated IRE1α-Dependent Decay (RIDD) [14,15]. Interestingly, the degree of oligomerization of IRE1 may define its RNase activity towards *XBP1* mRNA splicing or RIDD, ultimately impacting on cell fate (**Figure 1**). Although the order of oligomerization required for *XBP1* mRNA splicing vs. RIDD is still debated, there is a consensus on the cytoprotective effects of XBP1s and the dual protective or cell death-inducing outputs of RIDD under ER stress [16,17].

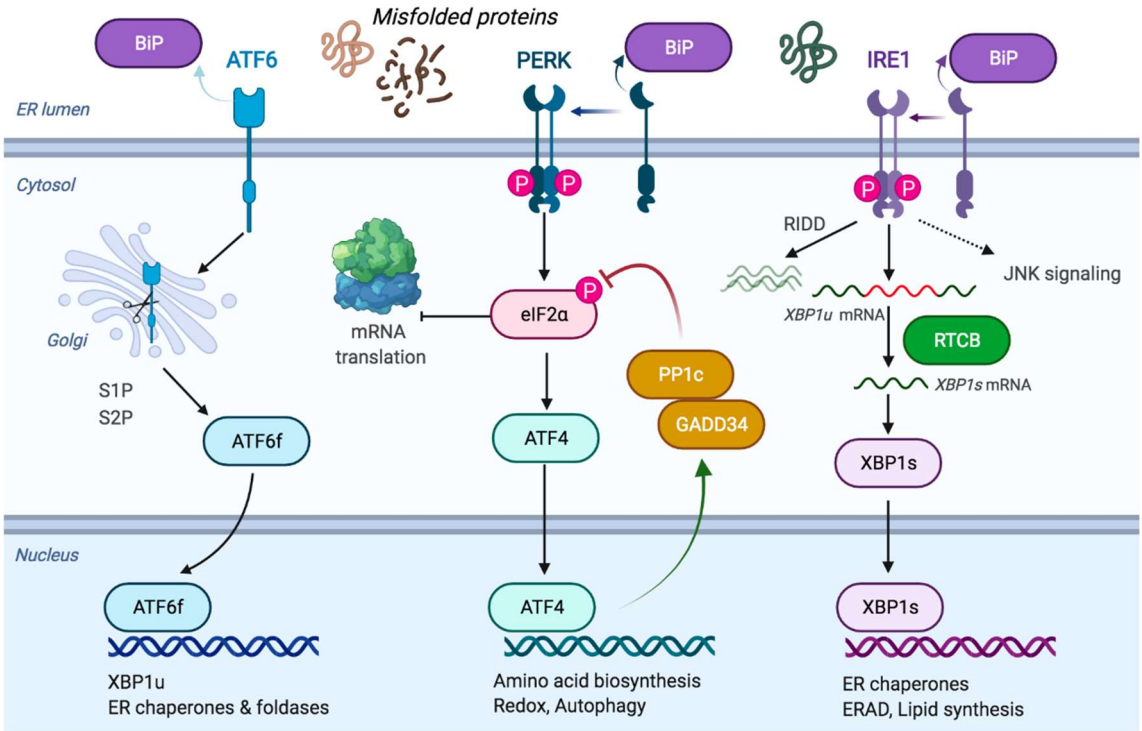

Figure 1. Schematic representation of the signalling pathways composing the Unfolded Protein Response.

In this model, while *XBP1* mRNA splicing is induced in the adaptive UPR (aUPR) and inactivated during the terminal UPR (tUPR), RIDD displays an incremental activation pattern reaching unspecific RNA degradation during tUPR. Despite our knowledge on IRE1 signaling biological outputs, little is known so far on how signals emanating from these two RNase activities do integrate. The existence of a multiprotein complex recruited in IRE1 foci that dynamically changes composition during the course of ER stress has been suggested as a possible modulation mechanism [18]. This is supported by the identification of IRE1 interactors regulating *XBP1* mRNA splicing differently than RIDD [19].

Over the past two decades, the key roles of IRE1 signaling in cellular adaptation to proteotoxic stress have also been linked to many pathophysiological conditions. IRE1 signaling was found to play critical functions in various degenerative disorders including for instance Parkinson's disease, Alzheimer's disease or Amyotrophic lateral sclerosis [20–25]. It was also found to play an important role in metabolic (e.g., diabetes, NAFLD [16,26] or inflammatory diseases [27,28] (e.g., Crohn's disease [29,30]). IRE1 signaling, either through *XBP1* mRNA splicing or RIDD, has also been shown to contribute to tumor development and to mechanisms of resistance to treatments [17]. As such, it has been proven that IRE1 could act as a relevant therapeutic target in multiple myeloma [31,32], acute myeloid leukemia [33], prostate [34], ovarian [35], triple negative breast [36,37], gastric [38–40], liver [41,42] cancers and primary brain tumors such as glioblastoma [17,43,44]. These discoveries sparked intensive efforts to identify small molecule modulators of IRE1 activity to be used as therapeutic tools in various diseases. Thus far, three major binding sites were identified, including the kinase pocket, the RNase pocket and the dimer interface [45]. In this review, we propose to focus exclusively on compounds targeting the kinase or RNase pockets, and for which structural data or structural-activity relationship studies are available. IRE1 kinase inhibition was the most popular strategy so far, and led to the identification of multiple chemical series with different mode of actions. To better understand the molecular basis of the small molecules modulating IRE1 activity presented in this review, some key concepts about kinase need to be reminded. Kinase inhibitors have been classified from type I to VI based on crystallographic data and key structural elements found in all kinases such as the DFG (Asp-Phe-Gly) motif, R-spine, activation segment and αC helix have been used to distinguish active and inactive kinases [46]. Type I, $I^{1/2}$ and II, which are the most

predominant, all bind into the adenine binding pocket where they form hydrogen bonds with the hinge residues that connect the small and large lobes, but differ by the protein kinase conformation bound. Thus, type I inhibitor bind fully active kinases (DFG in, αC in), type $I^{1/2}$ bind to a DFG in but inactive conformation, and type II bind to a DFG out inactive conformation. Type III and IV are allosteric inhibitors as they do not bind to the ATP binding site, but next to it or elsewhere entirely, respectively. The type V class encompasses more rare bivalent inhibitors. Finally, the recent emergence of covalent compounds that target the catalytic site prompted the creation of a novel type VI class [47]. The various types of IRE1 kinase inhibitors identified and developed prompted significant advancement in the understanding of IRE1 activation mechanism, but did not yet deliver any molecule able to enter the clinic. Regarding IRE1 RNase inhibition, several compounds were identified which required covalent binding to efficiently impair this catalytic activity. Although targeted covalent ligands are trending again [48], this characteristic is generally considered as unfavorable due to common occurrence of off-target effects/promiscuous binding. Nevertheless, one such covalent RNase inhibitor MKC8866 (renamed ORIN1001) entered clinical trial in association with Paclitaxel to target triple negative breast tumors (https://clinicaltrials.gov/ct2/show/NCT03950570). The modulation of IRE1 activity by small molecules currently represents a very active field of research as witnessed by the striking increase in patented inhibitors observed between 2018 and 2021 from numerous companies and academic laboratories (19 patents total, of which 16 were filed since 2017). In this review, beyond the extensive coverage of the molecular and structural mechanisms by which IRE1 kinase and RNase targeting molecules affect IRE1 functions, we will also briefly discuss on yet unexplored novel modalities to pharmacologically target IRE1 (PROTAC, PPIs, FBDD, etc.)[49]. Collectively, the work presented below is the first of its kind as it provides a synthetic, structural and molecular view of the mechanisms by which IRE1 modulators function, which could provide some hints on novel strategies to identify novel and more potent inhibitors.

IRE1 ATP-competitive activators

N^4-(1H-pyrazol-3-yl)pyrimidine-2,4-diamine: APY29 & IPA

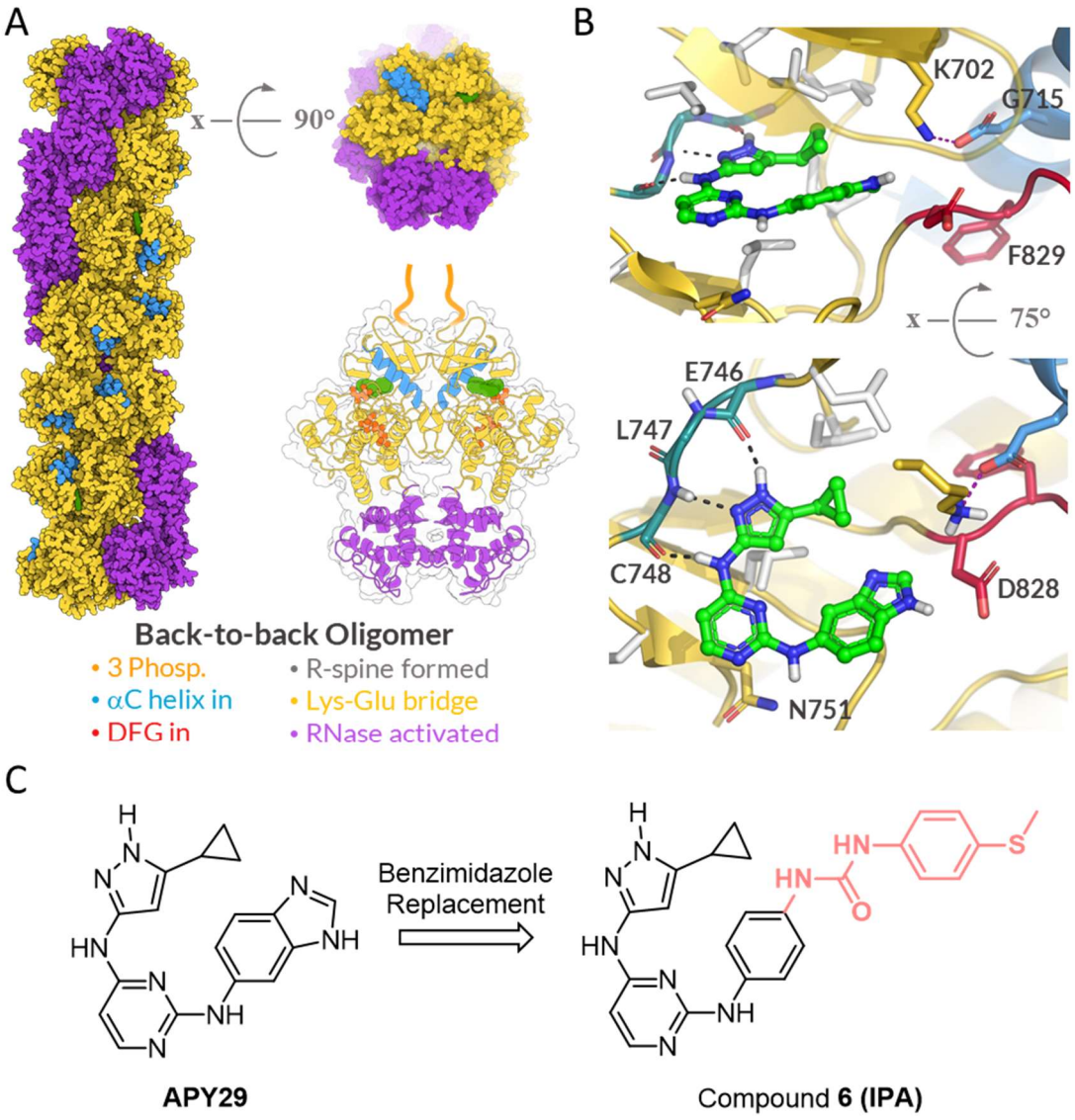

Figure 2. A. Graphical representation of the high-order oligomer structure of the *Saccharomyces cerevisiae* yeast IRE1 (*y*IRE1) cytosolic domain in complex with APY29 (PDB ID 3FBV) and constitutive back-to-back dimer (cartoon; ligand as green spheres; αC-helix in blue; Kinase C- & N-lobes in yellow; RNase domain in purple; Phosphorylated residues in orange). Key structural changes highlighted underneath. B. Front and top view of APY29 in the kinase pocket with key residues indicated (ligand as ball and stick with green carbon atoms; hydrogen bonds as dark gray dashed lines; salt bridge as purple dashed line; DFG motif side chains as red sticks; hinge backbone atoms as teal sticks; apolar residue as white sticks; αC-helix as blue cartoon and sticks). C. SAR optimization of APY29 by replacement of the benzimidazole moiety that led to compound 6, also known as IPA (for IRE1/PERK Activator). Structural changes highlighted in colors with bold bonds.

In their pioneering work on the exploration of IRE1 higher-order activation mechanism, Korennykh *et al.* reported the very first kinase site bound RNase activators, with notably a unique co-crystal structure of Saccharomyces cerevisiae yeast IRE1 (*y*IRE1) in complex with a synthetic ligand [22]. Their serendipitous identification of type I kinase inhibitors (Sunitinib, APY24 & APY29) capable of activating the *y*IRE1 RNase activity represented a major breakthrough and kickstarted the interest for IRE1 targeting kinase inhibitors. By combining the use of a specific *y*IRE1 construct capable of self-activating and self-assembling, the authors successfully obtained an oligomeric crystal structure representative of *y*IRE1 activated state with their most potent activator APY29 bound (Figure 2A) (PDB ID 3FBV). In this structure, the aminopyrazole core of APY29 forms three hydrogen bonds with the hinge residues Glu746 and Cys748 (Glu643 and Cys645 in *h*IRE1), anchoring strongly the ligand in the kinase pocket (Figure 2B). Additional Van der Waals interactions and probable hydrogen bonds with Asn751 and Asp828 (not visible in the crystal structure) complete the interaction patterns of APY29. This observed binding mode allowed to hypothesize on the superior potency of APY29 and APY24 over Sunitinib, a broad inhibitor of receptor tyrosine kinases (RTKs) and an approved anti-cancer drug (Sutent®). Whereas APY29 and APY24 are able to extend into the kinase pocket where the ribose-phosphate moiety of ADP normally binds along with its Mg^{2+} cofactor, Sunitinib opens more toward the solvent due to its different three-dimensional shape. The tight crystal packing of the *y*IRE1 also made possible the identification of unique structural features that helped decipher the IRE1 activation mechanism. Two new interfaces, not present in previous back-to-back dimer structure and dubbed $IF2^c$ and $IF3^c$, were identified and demonstrated to contribute to the control of IRE1 RNase activity. Most notably, the αD helix and the phosphorylated activation loop (pS840, pS841 & pT844) were fully visible in the $IF3^c$ interface and revealed that the activation loop extends into a partner kinase domain. Deeper analysis of this structure and its implication in IRE1 activation has been reviewed elsewhere [50].

A few years later, the same research group presented in a second publication [51], a small library of new molecules derived from APY29 and aimed at potently activating hIRE1 RNase function. The APY29 benzimidazole was replaced by a diphenyl urea moiety (Figure 2C) with various substitutions, a motif successfully used in the design of other kinase inhibitors [52]. The rest of the scaffold remained unchanged as it was clearly identified as essential to maintain affinity and key interactions. Among the ten analogues

synthesized, the *para*-substituted methyl thioether compound **6** was the most potent and activated by a 900-fold factor the IRE1 RNase *in vitro*. These changes in the structure also led to a major improvement in kinase selectivity, with only 16 kinases inhibited > 80% at 1µM (total panel of 266 kinases). Compound **6** was later renamed in the paper as **I**RE1/**P**ERK **A**ctivator, **IPA** (Figure 2C), as it was found to also activate the PERK signaling pathway at low concentrations, whereas inhibiting it at higher compound concentrations and the effect of combined alteration of both pathways remains to be characterized in cellular models of relevant diseases [51].

***Imidazo[1,2-b]pyridazine*: Compound 3**

In a landmark study (47), Joshi et al. reported the discovery of a second class of IRE1 RNase activators and were able to obtain an unambiguous ligand-bound crystal structure (Figure 3A) (PDB ID 4Z7H), along with an apo IRE1 structure (PDB ID 4Z7G).

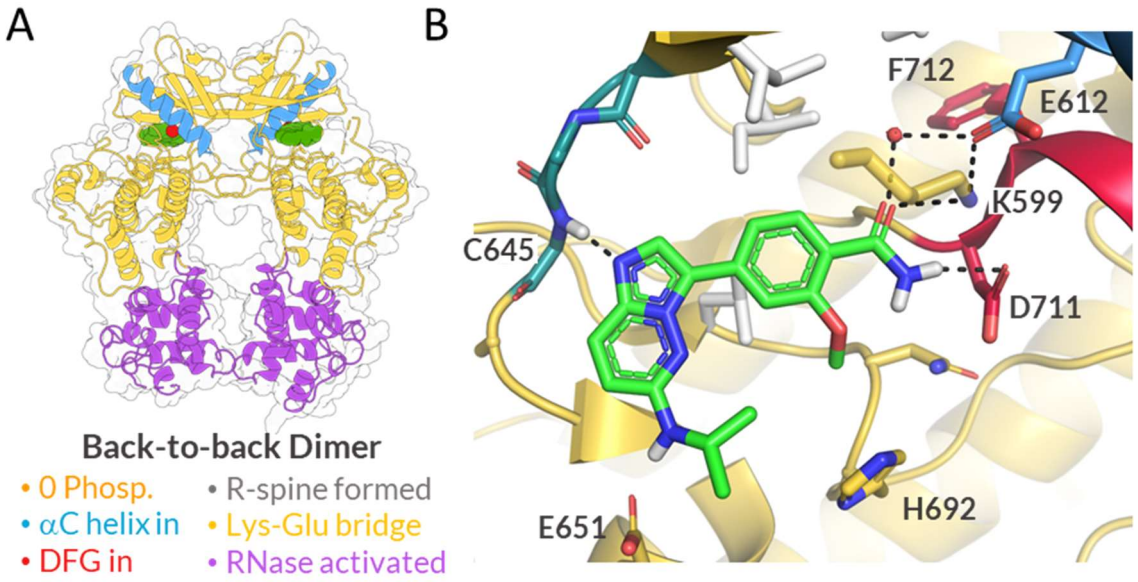

Figure 3. A. Graphical representation of the back-to-back dimer visible in the structure of *h*IRE1 in complex with compound 3 (PDB ID 4Z7H) with key structural changes highlighted underneath. B. Top view of 3 in the kinase pocket with key interaction and residues indicated. Color coding and representation as in Figure 2; red sphere represents an ordered water molecule bridging interactions with the protein.

These two novel snapshots of distinct IRE1 activation stages improved the understanding of the fine structural changes happening within the kinase domain during early IRE1 activation which are needed for RNase activity. The ligand, compound **3**, appears to have

been identified in a high-throughput screening campaign using a DELFIA assay developed by the authors [53], where it inhibited IRE1 autophosphorylation with an IC_{50} of 218 nM (± 150 nM). Its impact on IRE1 RNase activity was then assessed in a FRET-based assay using unphosphorylated IRE1 and the endoribonuclease function was potently enhanced (EC_{50} = 143 nM). Similarities in its binding mode can be drawn with APY29 [22], both type I kinase inhibitor residing in the adenine pocket (Figures 2B & 3B). As such, the usual interactions with hinge residues are present in the form of a single H-bond between the backbone N-H of hinge residue Cys645 and the ligand's imidazole *N*-1. Numerous Van der Waals interactions are also observed due to the nature of the surrounding residues and tight enclosing of the ligand in the kinase pocket. What differs from the APY29 binding mode is that the 2-methoxybenzamide reaches further towards the DFG motif and Lys-Glu bridge where it makes unambiguous hydrogen bonds. In particular, the amide NH_2 interacts with the Asp711 carboxylic acid group, while the amide carbonyl is engaged simultaneously with Lys599 and a buried water molecule is acting as a bridge to Glu612. Consequently, the conformation of the DFG motif is altered and, in particular, the Phe712 side chain shifts in position to fully form the R-spine, a prerequisite for RNase activation. Comparison of the ligand-bound and apo *h*IRE1 structures, and the APY29-oligomeric *y*IRE1 structure obtained by Korennykh *et al.* [22], supported the hypothesis that these ligands activate IRE1 RNase activity through the stabilization of an active conformation of the kinase site (DFG-in, αC helix in, R-spine formed).

***Naphtalenoxy-pyridyl-pyrimidine & Pyrazolo-pyridine*: G-9807 & G-1749**

At the end of 2020, researchers from Genentech published an impactful study [54] revealing the full extent of the interdomain regulation within IRE1 and how it can be controlled through minor changes in ligands' molecular structures that act as a switch of the bioactive conformation. The structural data obtained by Ferri *et al.* also shed light on the importance of the activation loop and of its phosphorylation in regulating RNase activation. In the continuation of their previous studies [31,55] and to elucidate further the principles governing IRE1 RNase activation, Ferri et *al.* set out to screen the internal Genentech chemical library to identify better kinase site binding ligand capable of activating IRE1 RNase function. To this end, an ATP-competitive TR-FRET assay was used a preliminary screen to identify kinase binders, then evaluated in IRE1-specific kinetic RNA cleavage assay. The most promising hits were then tested in KMS-11

multiple myeloma cells, known to hyper-produce immunoglobulins in the ER and therefore be strongly dependent on the IRE1 pathway to cope with the induced ER stress. Two distinct molecules were identified, **G-9807** and **G-1749**, which present a pyrazolo-pyridine and a phenoxy-pyridyl-pyrimidine scaffold, respectively (Figure 4). Of note, G-1749 is a structurally close analogue of earlier identified RNase inhibitor KIRA8. These compounds performed extremely well in all assays, G-9807 showing a 3.50-fold increase in RNase activity *in vitro* and a 7.21-fold increase in *XBP1*s mRNA levels in cells. Similar results were found for G-1749 with a 1.86-fold and 8.26-fold increases, respectively. Kinase selectivity was also assessed and at 1µM, G-1749 only inhibits 6 out of the 218 kinases constituting the panel (undisclosed for G-9807) and none of the compounds significantly affected PERK, even at a high concentrations (1 mM).

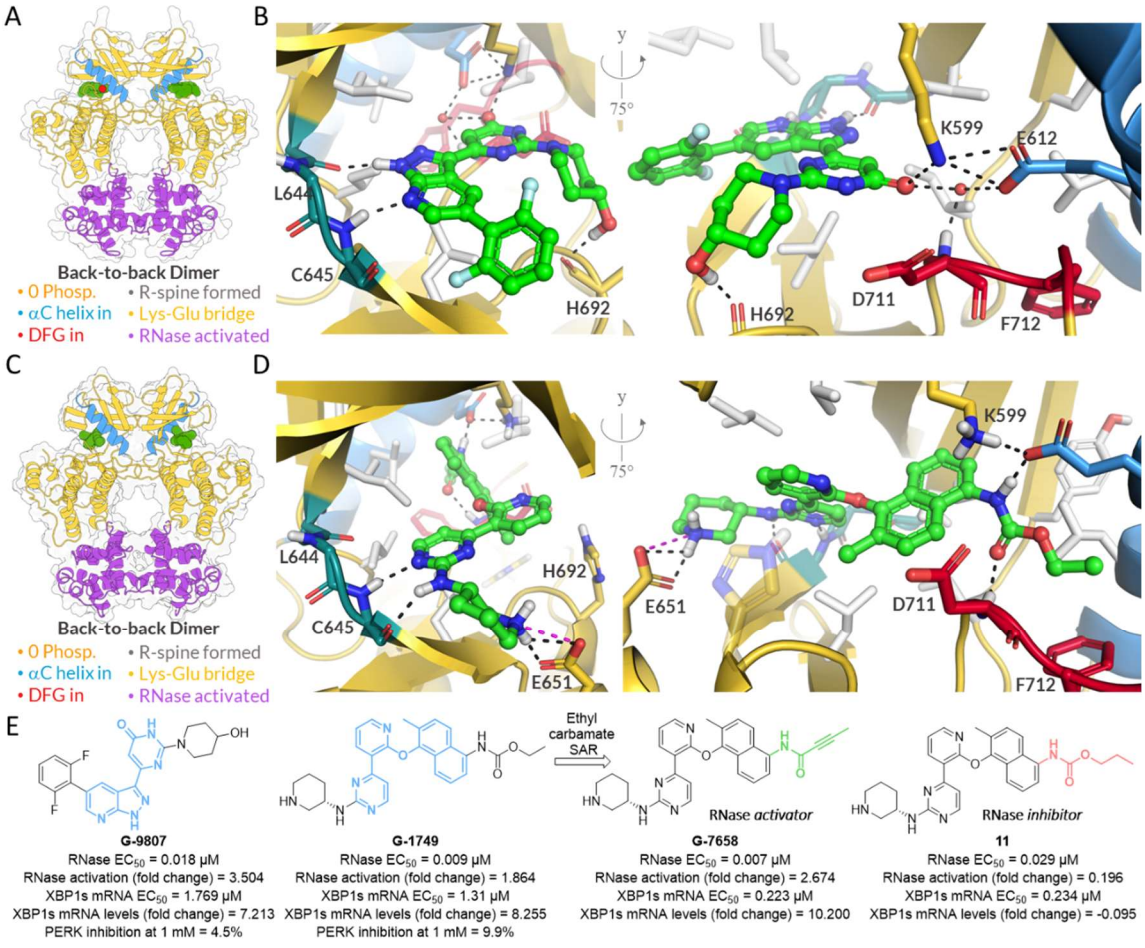

Figure 4. Graphical representations of the back-to-back dimer visible in the structure of human IRE1 (*h*IRE1) cytosolic domain in a complex with A. compound G-9807 (PDB ID 6W3K) and C. compound G-1749 (PDB ID 6W39), with key structural changes highlighted underneath. B. Left-side and right-side views of B. G-9807 and D. G-1749 in the kinase pocket with key interaction and residues indicated. Color coding and

representation as in Figure 2; red sphere represents an ordered water molecule bridging interactions with the protein. E. SAR study of the ethyl carbamate 'tail' of G-1749. Modulation around the nature and size of the tail led to the but-2-ynamide-substituted *RNase activator* G-7658 (PDB ID 6W3A), and 4,4-dimethylpent-2-ynamide-substituted *RNase inhibitor* 11.

Using sedimentation velocity analytical ultracentrifugation experiments, the authors demonstrate that G-9807 is able to stabilize a dimeric form of unphosphorylated human IRE1 (*h*IRE1) cytosolic domain, similarly to previous RNase activators APY29 [22] and compound **3** [56], whereas G-1749 does not, underlying differences in activation mechanisms. Each ligand was then successfully co-crystalized in complex with unphosphorylated *h*IRE1 to gain structural insights into this disparity (PDB IDs 6W39 & 6W3K), complemented by hydrogen-deuterium exchange (HDX) experiments to study the protein conformation in solution. Both the G-1749 and G-9807 crystal structures show IRE1 in an activated conformation, with all the hallmark of an active kinase in complex with a type I kinase inhibitor (Figures 4A & 4C). Regarding the ligands' binding modes, the usual key hydrogen bonding with the hinge residues, and in particular Cys645, are observed with the pyrazolopyridine motif of G-9807 and the aminopyrimidine ring of G-1749 (Figure 4B& 4D. The 4-hydroxypiperidin-1-yl of G-9807 makes an unseen before hydrogen bond to the backbone carbonyl of His692. The main differences between the two ligand binding modes lie in their interactions with the DFG residues and Lys-Glu bridge. Whereas G-9807 interacts with Glu612 through a buried water molecule and Lys599 (Figure 4B), G-1749 makes a direct hydrogen bond with Glu612 via the carbamate NH. However, the true novelty was found in the structure of G-1749, where the ethyl carbamate 'tail' of the ligand is not observed in the back pocket as seen with the chlorophenyl moiety of KIRA8, but rather wedges itself in a front pocket underneath the αC-helix and along the DFG residues, thus sparing the Lys-Glu bridge. As a consequence, G-1749 appears to force the activation loop in an upward conformation, later confirmed by the HDX analysis. This unique feature differentiates G-1749 from previously published activators and from G-9807.

A short SAR study on this tail was thus conducted and showed that the chemical substituents tolerated by the front pocket are very limited, where minor structural changes such as the elongation of the alkyl chain by one carbon (compound **11**, Figure 4E) or substitution of the carbamate oxygen atom by a methylene led to a complete reversal of

activity. Substituents not fitting the front pocket revert back to filling the back pocket, thus breaking the Lys-Glu bridge and displacing the αC-helix and acting as a switch from allosteric activation to inhibition. The most potent activator identified in the SAR study was the but-2-ynamide-substituted G-7658 (Figure 4E), which was successfully co-crystallized (PDB ID 6W3A) and showed near perfect overlap with G-1749. The upward conformation of the activation loop upon occupation of the front pocket prompted the authors to investigate the influence of its phosphorylation on ligand potency. By using precise phosphorylated IRE1 constructs in a combination of techniques and assays, the authors were able to demonstrate that the ability of G-1749 and its analogues to allosterically activate the RNase is highly dependent on the phosphorylation state of IRE1. In particular, they could pinpoint the interaction between pSer729 and Arg687 as a central component to this modulation switch. This contact rigidifies the activation loop in an extended and inactive configuration, thus making the conformational changes needed for ligand-induced activation energetically unfavorable. To sum up, this structurally driven study by Ferri *et al.* provides crucial insights into the kinase-RNase interdomain regulation happening within IRE1 upon ligand-binding by allosteric regulators and finally gives the tools to explore IRE1 activation strategies in a variety of diseases, and in particular cancer [49].

IRE1 ATP-competitive inhibitors

Imidazo[1,5-a]pyrazin-8-amine based inhibitors: **KIRA3, KIRA6 & KIRA7**

By observing the binding mode of ATP-competitive type I inhibitor APY29 and its allosteric role in activating IRE1 RNase function, Wang et *al.* hypothesized that development of type II inhibitors that stabilize the IRE1 kinase domain in an alternative inactive conformation could result in the opposing effect on the endoribonuclease activity, thereby fully inhibiting the dual activities of IRE1 [57]. Based on this hypothesis, screening was carried out with a variety of type II kinase inhibitors know in the literature to induce a DFG-out motif. Only one ligand, compound **1**, showed inhibitory activity in the FRET-based RNase assay used for the screening. It was predicted, using Src co-crystal structure, that the pyrazolopyrimidine motif of **1** could display similar interactions as APY29 with the IRE1 hinge motif (Figures 5A & 5B), but its conformation in the binding site has been shown to stabilize the DFG-out conformation [58].

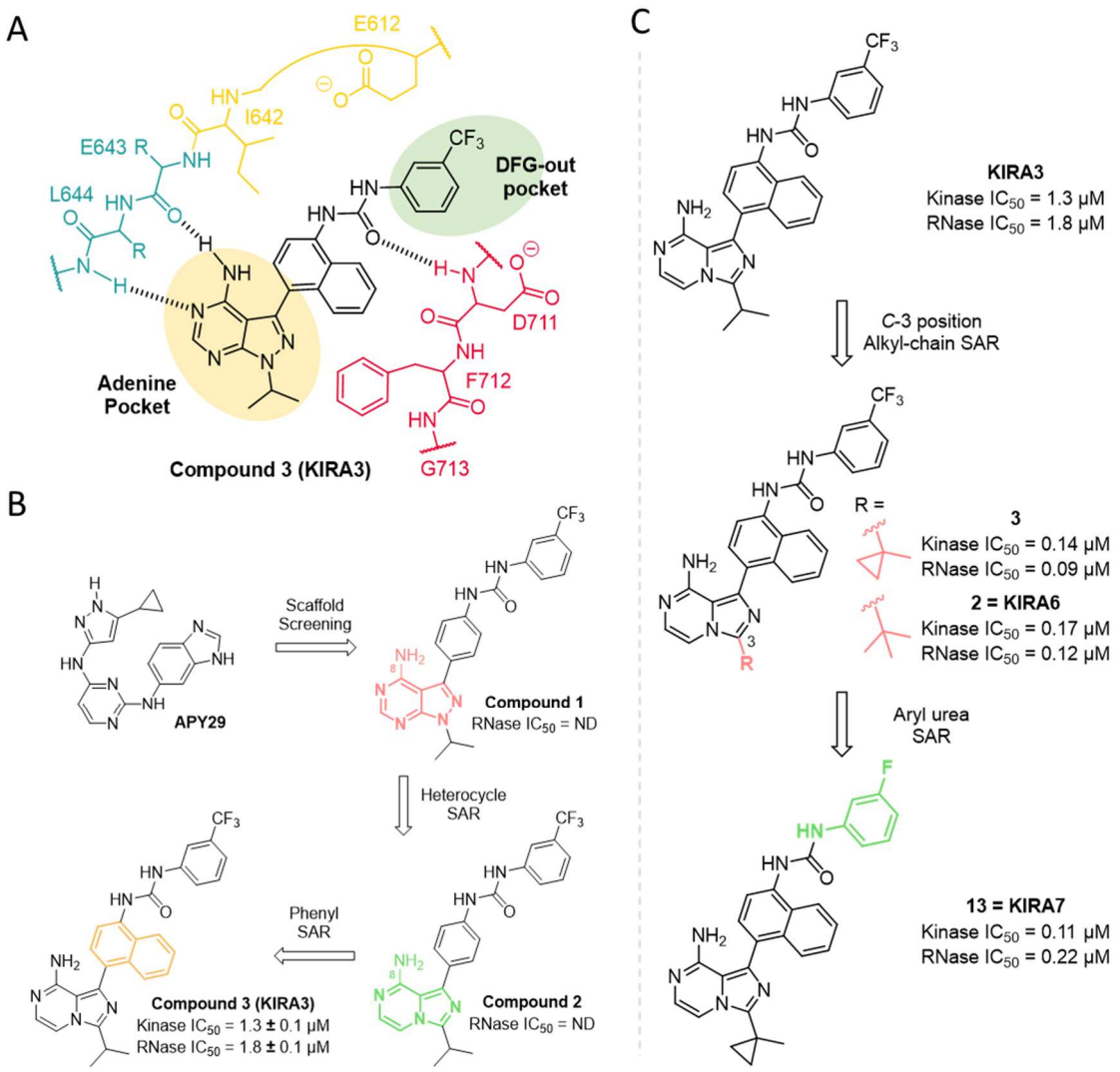

Figure 5. A. Proposed binding mode of compound 3 in *h*IRE1 kinase pocket in the absence of a crystal structure (color coding as in Figure 2; H-bonds as dashed dark gray lines) B. Discovery of Compound 1 from APY29 by scaffold screening and following structural optimizations through SAR studies that led to compound 3. Structural changes highlighted in colors with bold bonds. C. Structural optimizations through SAR studies of the *C*-3 position and aryl urea that led compound 2, 3 and ultimately 13. Structural changes highlighted in colors with bold bonds.

Despite its modest activity at 20 and 60 µM concentrations, compound **1** was used as a starting point for SAR and most of the modifications (undisclosed) did not give positive results except for the replacement of the 1*H*-pyrazolo[3,4-*d*]pyrimidine scaffold by an imidazo[1,5-*a*]pyrazine core, yielding compound **2** (Figure 5B). Two hydrogen bonds are formed with the hinge region (Glu643 to Cys645); between the aromatic amine of **1** and the carbonyl of Glu643, and between a nitrogen of the pyrimidine part of the

imidazopyrazine core with the next peptide bond between Leu644 and Cys645. The rest of the imidazopyrazine core occupies the adenine pocket. Moreover, replacing the 4-anilino group with a naphthylamine group in the C-3 position provided the most potent ligand **3** (Figure 5A).

According to the authors model, the naphthyl group can adopt an orthogonal conformation with the imidazopyrazine moiety. The naphthyl rings stacks against the Ile642 gatekeeper residue. The hydrophobic pocket, created by DFG-in/out movement of the Phe712, is filled by the *meta*-trifluoromethylphenyl substituent. Compound **3** has an inhibition capacity on the kinase activity IC_{50} = 1.3 μM and 1.8 μM on RNase activity. In line with their starting hypothesis, the authors also demonstrated through the study of alkylation rates of three exposed cysteine residues (Cys572, Cys645 and Cys715), in the presence or absence of ligand, that **APY29** and **3** share the same binding site, despite exerting opposing effects. Unlike the other two cysteines, Cys645 is highly shielded from the alkylating agent in both cases due to its direct interactions with the ligands. Additionally, it was observed that the two inhibitors exert opposing effects on the accessibility of Cys715, located on the activation loop of IRE1 near the C-terminal DFG-motif. Compound **3** increased the rate of alkylation whereas **APY29** decreased it. In consequence, the activation loop will adopt different stabilized conformations. To validate their binding model, the authors generated two closely related analogues of **3**, aptly named **4** and **5**, bearing key structural modifications expected to make them inactive. Compound **4** was *N*-methylated on 8-position which would disrupt the hydrogen bond interaction with Glu643's carbonyl. Regarding **5,** the urea connecting the naphthyl and the trifluoromethylphenyl group was replaced by an amide function, intended to reduce hydrogen bonding with the DFG motif and the favorable interactions with the hydrophobic pocket created by its movement (Figure 5A). Consistent with their predictions, both **4** and **5** showed a loss of potency in the RNase assay. With this study, the authors demonstrated the possibility to inhibit RNase activity of IRE1 with type II kinase inhibitors and gave keys to generate more potent compounds. Compound **3**, later referred as **KIRA3** in recent literature, served as the starting point for further optimization studies.

Four years after the initial report on the discovery of compound **3**, Feldman *et al.* published a follow-up paper [59] in which a series of derivatives, named KIRAs for **K**inase **I**nhibiting **R**Nase **A**ttenuators, were developed and tested to provide insight into the allosteric relationship between the kinase and RNase domains (Figure 5C). In

particular, a SAR study was conducted to better understand how specific interactions between the inhibitor and the ATP-binding site regulate IRE1 RNase activity. In the absence of structural data, four series of analogues were synthesized for evaluation using **KIRA3** as a benchmark. Firstly, a modification of alkyl groups R_1 was done in the C-3 position of the imidazopyrazine group. Compared to KIRA3, both kinase and RNase activities were better for all these analogues. In particular, replacement of the isopropyl group with *tert*-butyl (**2**) and cyclopropylmethyl (**3**) improves the kinase IC_{50} from 1.3 µM (**1**) to 0.17 µM for **2** and 0.14 µM for **3**. Regarding RNase IC_{50}, this modification of the alkyl side chain allowed a 15-fold decrease for **2** and 20-fold for **3** settling down to 0.12 µM and 0.09 µM, respectively. The cyclopropylmethyl was deemed the most optimal alkyl substituent and retained for the continuation of the study. The second series of modifications investigated the replacement of the naphthyl group with various substituted phenyl rings. None of these new analogues showed improved potencies compared to **3**. Only compound **7** with a 3-fluorophenyl as R_2 group maintained sub-micromolar activities, but still lower by a factor of 6 and 4 in the kinase and RNase assays, respectively. As a consequence, the naphtyl group was kept for further modulation.

Next, the aryl and urea domains were modified (series 3 and 4) to evaluate their importance on the stabilization of the DFG-out motif and on the ensuing allosteric inhibition of the RNase domain. These targeted modifications were motivated by the assumption that the aryl-urea moiety found in all KIRAs is thought to be responsible for inducing a DFG-out conformation of the kinase upon binding. The aryl group could then occupy a newly created hydrophobic pocket formed by displacement of the αC-helix and the Phe712 side chain. This is supported by the fact that this pharmacophore is found in many type-II inhibitors [60] and is known to stabilize the inactive DFG-out conformation [61]. Eleven diverse 3- and 4-substituted phenyl groups were accepted and tolerated, but only the 3-fluorophenyl substituted compound **13** showed equivalent potencies to **3**; the other twelve analogues wavering around 0.30/0.35 µM for kinase IC_{50} and 0.20/0.30 µM for RNase IC_{50}. The authors have also shown the possibility to incorporate a 4-methylpiperazin-1-yl group, a part of a clinically approved drug imatinib, on position 4 of the aryl group without loss of potency. Analogues bearing substituents like benzyl, heteroaryl or cycloalkyl instead of aryl were poor inhibitors, with smaller rings showing the most important decreases in RNase potency, which might be due to only partial displacement of the DFG motif and αC-helix. Finally, the crucial role of the urea linker for allosteric inhibition of the RNase activity *via* the formation of hydrogen bonds was

confirmed, since masking of one the *N*-H with a methyl group induced a ~200-fold loss in potency, and full loss when both hydrogens were hidden in an imidazolidinone group. At the end of the study, two products were considered interesting in regards to their kinase and RNase IC_{50s}, compounds **7** and **13**, later renamed **KIRA6** and **KIRA7**, respectively. In cells, **KIRA6** demonstrated good allosteric inhibition of the IRE1 RNase activity and promoted cell survival under ER stress [62]. **KIRA7** has been shown to decrease terminal UPR signaling and prevents fibrotic effects in mice lungs [63].

Pyrimidyl-pyridyloxy-naphtyl sulfonamide: KIRA8

Dissatisfied with the potency and/or selectivity of the available IRE1 inhibitors at the time, Harrington *et al.* [64] performed a high-throughput screening of the Amgen small-molecule library to find better molecules with preclinical profile and that could be used as a tool to validate that tumor cells with a high protein synthesis burden would be driven to apoptosis in the absence of this survival pathway. The primary screening consisted of an *in vitro XBP1* mRNA stem-loop cleavage assay to identify IRE1 RNase inhibitors, regardless of the binding site, and a cellular XBP1-luciferase assay was used as a secondary readout. Selectivity against JNK3 kinase, structurally close to IRE1, was also monitored. Compound **1**, a pyrimidinyl-pyridyloxy-naphtalene bearing a benzimidazole moiety (Figure 6A) was identified through this HTS campaign as an IRE1 kinase and RNAse inhibitor (IRE1α IC_{50} = 71 nM, XBP1-Luc IC_{50} = 270 nM).

However, 1 exhibited a moderate kinase selectivity profile with 17 kinases inhibited out of 442 (at 1μM, percent of control (POC) < 35), among which figure the Jun and Aurora kinases that could complexify the efforts to validate IRE1 as a target for oncology. The authors thereafter undertook a hit-to-lead strategy on the basis of compound **1** to improve selectivity and RNase inhibition. Using knowledge gained in their previous work on Aurora kinases with similar analogues, a methyl group was first introduced in the *ortho* position of the ether link to lock its rotation. The methylated compound **2** exhibited a 5-fold increase in IRE1 RNase inhibition (IC_{50} = 14 nM), but most importantly showed increased selectivity against Aurora (IC_{50} > 50 μM) and JNK3 (IC_{50} = 0.71 μM) kinases. In the meantime, the authors also modulated the amine side chain of the pyrimidine ring of 1 to study its influence on inhibition and selectivity. Replacement of the basic nitrogen of the tertiary amine by an aliphatic isopropyl led to a complete loss of activity and selectivity. Introduction of a hydroxyl group resulted in a 2-3-fold loss in potency towards

IRE1 while increasing ten-fold JNK3 inhibition, resulting in a reversal of the compound's selectivity.

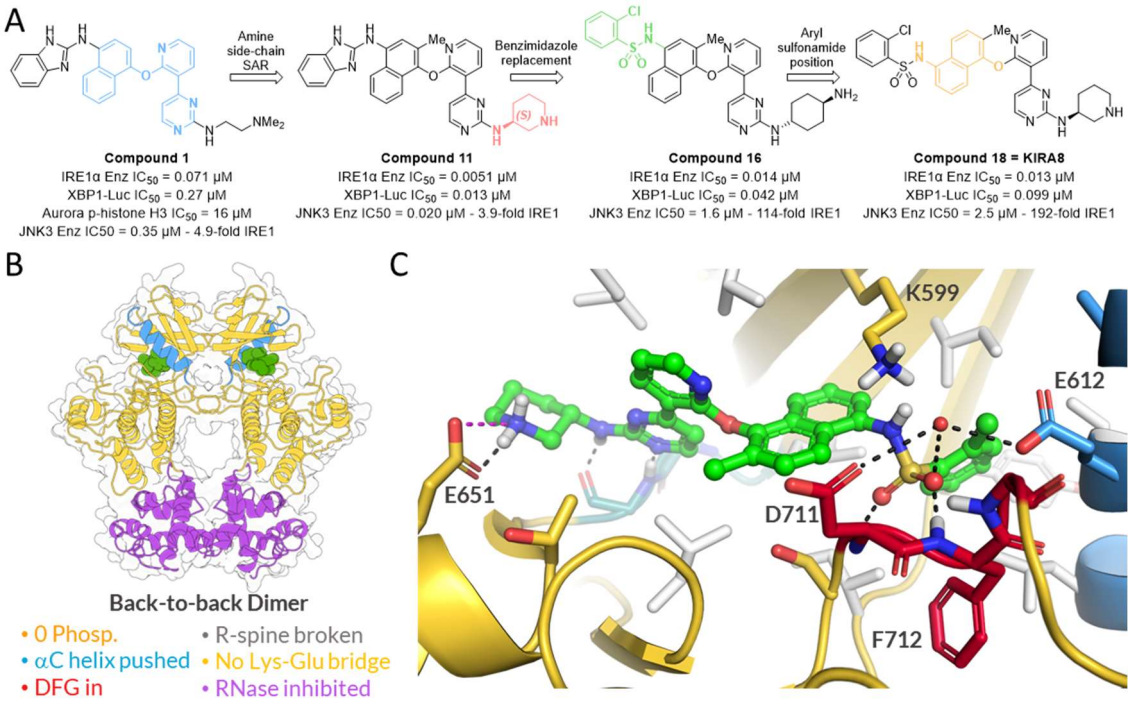

Figure 6. A. Successive structural optimizations and key intermediates that led to compound 18 (KIRA8). Structural changes highlighted in colors with bold bonds. B. Graphical representation of the back-to-back dimer visible in the structure of *h*IRE1 in complex with compound 18 (PDB ID 6URC). Key structural changes highlighted underneath. C. Front view of compound 18 in the kinase pocket with key interaction and residues indicated. Color coding and representation as in Figure 2; red sphere represent an ordered water molecule bridging interactions with the protein.

These first results highlighted the need for basic nitrogen to maintain selectivity and good levels of IRE1 inhibition, later rationalized later by a co-crystal structure (Figure 6B & 6C). Piperidines and cyclohexylamines were next investigated as cyclic surrogates. Inhibitory activity of racemic methyl-piperidine was nearly similar to 1, despite a lower selectivity against JNK3 (0.005 μM *vs* 0.35 μM for 1). Interestingly, the *(S)* stereochemistry was found to be 5-fold more active toward IRE1 than the *(R)* and to increase selectivity against JNK3. Similar observations were made in the cyclohexanediamines serie, where the cis-isomer was 4-fold less active but maintained similar selectivity against JNK3. Together, these results showed the importance of the stereochemistry, and therefore conformation, of this substituent to preserve potency.

Compounds **11** (Figure 6C), bearing simultaneously the *(S)*-3-aminopiperidine and additional methyl on the naphthyl ring yielded excellent IRE1 RNase inhibition (IC_{50} = 0.0051 μM), but was still too active on JNK3 (IC_{50} = 0.020 μM). To mitigate the selectivity issue against JNK3, efforts were next turned toward replacement of the benzimidazole ring. Its replacement with a benzoxazole moiety did not have a significant impact on potency or JNK3 selectivity. In contrast, introduction of a phenylsulfonamide resulted in a significantly increase in selectivity (49-fold). Substitution at the ortho position of this arylsulfonamide with an electron donating group (methoxy) had minimal influence, whereas electron withdrawing moieties (nitrile or chloro) resulted in more potent compounds in vitro and in cells. Significant selectivity improvement were also observed, and in particular for the *ortho*-chlorophenyl compound **16** (114-fold, Figure 6C).

The obtention of a co-crystal structure of arylsulfonamide analog 16 bound to dephosphorylated human IRE1α (PDB ID 4U6R) allowed to identify some critical interactions (Figure 6B). These data revealed that the ortho-chlorophenylsulfonamide disrupt the Lys-Glu bridge, pushes outward the αC-helix by around 2 Å, making way for the aryl ring to wedges itself in a newly formed αC-helix back pocket. The sulfonamide group makes two hydrogen bonds with the backbone *NH* of Asp711 and Phe712 of the DFG motifs, and proximity with Lys599 (3.1 Å) suggests that the sulfonamide *NH* is deprotonated in the bound state. The crystal structure also rationalized the importance of a controlled stereochemistry observed in cyclohexanediamine and piperidine substituted compounds as these can make a salt bridge with Glu651 if their stereochemistry allows it. Finally, observation of the binding mode of 16 provided insight for further structural optimizations that ultimately led to compound **18**, a potent and most selective candidate of the study with a RNase IC_{50} of 0.013 μM and a 192-fold increase in selectivity against JNK3. Compound **18**, later referred as **KIRA8** in the literature, was obtained by displacement the arylsulfonamide group from position 4 to 5 of the naphtyl moiety, and then replacement of the trans-cyclohexanediamine side-chain with the *(S)*-3-aminopiperidine to account for the shift in position in the kinase pocket. A crystal structure of KIRA8 in complex with *h*IRE1 (PDB ID 6URC) (Figure 6B & 6C) as obtained by Ferri and coworkers [54] surprisingly showed the protein in a back-to-back dimer, in contrast to the structure obtained with compound 16 that showed IRE1 as a monomer and was coherent with an outward swing of the αC-helix that could prevent dimerization/oligomerization. According to Ferri *et al.*, the dimer observed in the KIRA8

structure might be an artefact of the high protein concentration in the crystallization conditions. Finally, KIRA8 represented one of the first lead-like compound targeting IRE1 and as such served as the basis for further structural improvements, either to study the paralog-specific function of IRE1 [65] or to study IRE1 inner activation mechanisms [54].

2,8-diazaspiro[4.5]decane: GSK2850163

High-throughput screening of the GlaxoSmithKline compound collection in a phosphorylated IRE1 RNase activity assay led to the identification of GSK2850163, a potent and selective dual inhibitor of the IRE1 kinase (IC_{50} = 20 nM) and RNase activities (IC_{50} = 200 nM) presenting an original diazaspiro scaffold [66]. Subsequent protein crystallography efforts by the authors allowed them to obtain cocrystal structures of a triply phosphorylated IRE1 in complex with the endogenous ADP-Mg^{2+} ligand (PDB ID 4YZD), GSK2850163 (PDB ID 4YZ9), and broad kinase inhibitor staurosporine (PDB ID 4YZC), in all cases with IRE1 in a back-to-back dimer conformation (Figure 7A).

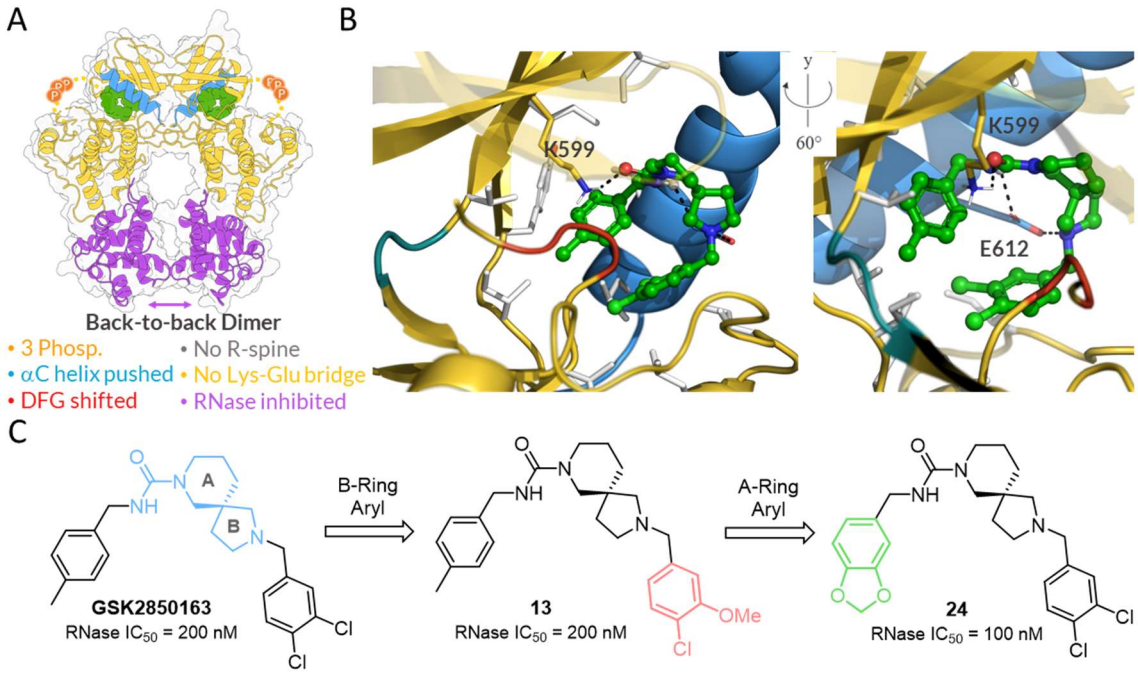

Figure 7. A. Graphical representation of the back-to-back dimer visible in the structure of *h*IRE1 in complex with GSK2850163 (PDB ID 4YZ9). Key structural changes highlighted underneath. B. Right-side and left-side view of GSK2850163 in the kinase site with key interaction and residues indicated. Color coding and representation as in Figure 2. C. Structural optimizations of the B-ring and representation of the most potent

analogue, compound 13, followed by A-ring modulation and obtention of 24. Structural changes highlighted in colors with bold bonds.

These structures revealed GSK2850163 as a type III kinase inhibitor [46] bound in an unusual fashion in the kinase pocket (Figure 7B). In contrast with other IRE1 modulators binding to this domain, GSK2850163 does not make any interactions with the hinge residues (Glu643; Lys644; Cys645) and actually sits ~12 Å away near the αC-helix. This binding event disrupt the conserved salt bridge between the αC-helix Glu612 and active site Lys599, which is needed to coordinates the α- and β-phosphate groups of the ATP molecule [67], thereby locking αC-helix in an inactive 'out' conformation. Ligand binding also pushes outward the DFG motif and disordered kinase activation loop by nearly 180° (further confirmed by HDX experiments). This results in the DFG motif occupying the ATP-binding site while GSK2850163 lies in the hydrophobic pocket previously occupied by Phe712 of the DFG motif. There, the ligand adopts a U-shaped conformation and interactions with the side chains of Glu612 and Lys599, a key catalytic residue, are described. Surprisingly, the nitrogen of the pyrrolidine ring of the 2,8-diazaspiro[4.5]decane is unprotonated in the original structure, despite being its most likely state at physiological pH and yielding an additional salt bridge with Glu612. The likely presence of a π-cation interaction between the tolyl group of GSK2850163 and the amine of Lys599 is also not discussed. Of note, only the *R*-enantiomer fitted the ligand electronic density and showed RNase inhibitory activity. Binding of GSK2850163 in the kinase back pocket is also observed to induce conformational changes throughout IRE1, resulting in an altered dimer interface and notably, an increased distance (~4 Å) between the RNase domains that would, together, disrupt its mRNA splicing ability.

To support the observed binding mode and improve further the ligand, concise SAR studies were carried out (Figure 7C), starting with the modulation of the NH of the urea and pyrrolidine nitrogen to investigate the importance of their hydrogen bonds with the carboxylic group of Glu612. Both proved to be critically important to maintain the compound's potency, with any change altering their hydrogen bonding capabilities drastically reducing RNase IC_{50s}. Next, the authors focused on modulating the two aryl moieties connected to each ring of the 2,8-diazaspiro[4.5]decane core, coined A and B, and that are nicely accommodated by the lipophilic environment of the pocket (Figure 7B). Substitution of the 3,4-dichlorophenyl group connected to the pyrrolidine B-ring by

a more polar aromatic ring such as a pyridine was not tolerated. Interestingly, individual removal of the chlorine atoms revealed that the 4-chlorobenzyl analogue has an IC_{50} only two times higher, 400 nM, highlighting the importance of the *para* position over the *meta*. Based on this observation, methyl and trifluoromethyl substituents were tried on this position but did not yield improvements. Modulation of the *meta* position with small lipophilic functional groups (*-F, -CH_3, -OCH_3*) was overall well tolerated and afforded equally potent ligands, with the exception of the bulkier trifluoromethyl group which showed loss in potency. Similar to what was observed with the B-ring aryl, replacement of the tolyl group attached to the A-ring urea by more polar pyridines led to a 30-to-60-fold loss in potency. Deletion or replacement of the *p*-methyl group by small lipophilic functions (*-Cl, -CH_3, -OCH_3*) afforded compounds with similar potency, but none better than the original hit. Lastly, the authors conclude their SAR study by presenting **24**, a benzo[*d*][1,3]dioxole analogue, which exhibit an RNase IC_{50} of 100 nM, a moderate two-fold improvement over GSK2850163. This study successfully identified a novel and potent dual IRE1 kinase/RNase inhibitor and characterized precisely its mode of action through a combination of X-ray protein crystallography and HDX experiments. Ligand optimization proved to be challenging, as demonstrated by the limited success of their SAR. To conclude, despite its unique binding mode among IRE1 modulators, its excellent kinase selectivity, nanomolar potency, and efficacy to in multiple myeloma cell lines, this class of compounds was not developed further, nor patented, by Glaxo Smith Kline for undisclosed reasons.

Imidazo[1,2-b]pyridazin-8-amine: **Compound 31**

Following up on their previous work on **Compound 3**, an IRE1 type I kinase inhibitors/RNase activator based on a 4-(imidazo[1,2-*b*]pyridazin-3-yl)benzamide scaffold, the Collins group recently reported the discovery of close structural analogues based on the imidazo[1,2-*b*]pyridazine-8-amine motif and capable of inhibiting the dual IRE1 activity (Figure 8) [56]. A scaffold screening on **Compound 3** led to the discovery of an analog, **2**, inhibitor of both the kinase (IC_{50} = 303 nM) and RNase functions (IC_{50} = 8.90 μM), suggesting a different allosteric effect on the RNase compared to typical type I IRE1 kinase inhibitors [68]. A crystal structure of **2** bound to IRE1 was obtained by compound soaking in IRE1-apo crystals and showed unusual structural changes throughout the IRE1 kinase domain (Figure 8A) (PDB ID 6HX1). Strong disordering of the αC-helix was observed, accompanied by an unusual folding of the first half of the

activation segment (res. 711- 726, [69]) in an antiparallel double β-strand, thus enclosing the ligand in a tight pocket. Most notably, the DFG motif was in an original intermediate conformation, termed DFG-up by the authors, and the Tyr628 residue normally in an up conformation is pointing downward. Looking at the ligand, the imidazo[1,2-*b*]pyridazine *N*-1 and 8-NH makes hydrogen bonds with the respective functions *NH* and CO of the hinge residue Cys645 (Figure 8B). An additional H-bond between the indazole *NH* and Tyr628 is also observed.

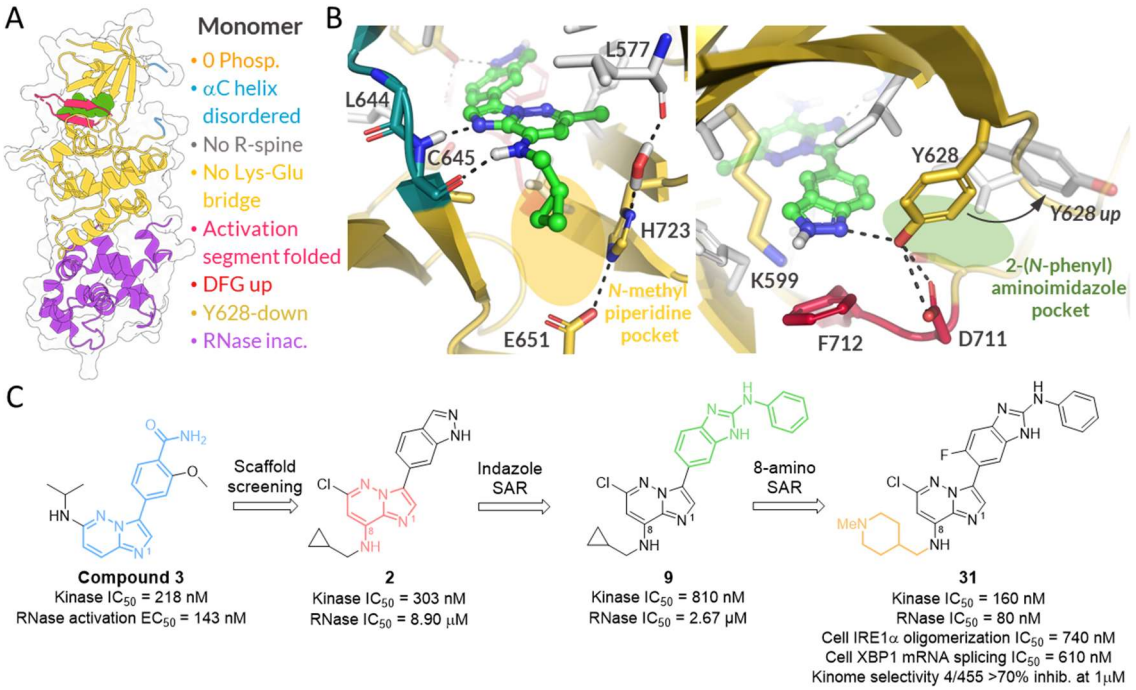

Figure 8. A. Graphical representation of the monomer visible in the structure of *h*IRE1 in complex with compound 2 (PDB ID 6HX1), precursor of compound 31. Key structural changes highlighted on the right-side. B. Left-side and right-side view of compound 2 in the kinase site. Key interactions and residues indicated as well as the likely position of the *N*-methyl piperidine (tan ellipse) and 2-(*N*-phenyl)aminoimidazole (green ellipse) moieties of 31. Color coding and representation as in Figure 2. C. Structural optimizations of compound 3 through scaffold screening and SAR studies on the indazole moiety and aromatic amine in C-8 that led to lead compound 31. Structural changes highlighted in colors with bold bonds.

Moreover, this compound was screened on the large Discover X KinomeScan panel and revealed an already significant selectivity with >70% inhibition of only 26/455 wild-type and mutant kinases. To optimize the inhibition, the role of each substituent was investigated by carrying out a structure-activity relationship around **2** (Figure 8C). In

particular, the indazol-5-yl substituent was replaced by several heterocycle scaffolds. The *N*-Methylated as well as the regioisomer (1*H*-indazol-4-yl) analogues showed the importance of the 1-*H*-indazol-5-yl group to maintain the inhibitory activity. The *N*-unsubstituted benzimidazole-5-yl analog exhibited a weaker kinase activity (> 10 μM) and no RNase inhibition. In spite of these results, further substitution of the benzimidazole at the C-2 position were explored. In particular, the (*N*-phenyl)-2-aminobenzimidazole motif was envisaged as being an isostere for the diaryl urea motif which is commonly found in type II kinase inhibitors [52]. Compared to compound **2**, the 2-(*N*-phenyl)amino benzimidazole **9** had a similar kinase activity (IC_{50} = 810 nM) but improved IRE1 RNase activity (IC_{50} = 2.67 μM). *N*-Alkylation at any position of this substituted benzimidazole framework (N1, N3 and NHPh) drastically reduced the potency (>10 μM), indicating that the 2-(*N*-phenyl)aminoimidazole functionality is probably involved in multiple hydrogen bonds. Finally, the replacement of the 8-(*N*-cyclopropylmethyl)amino substituent on the imidazo[1,2-*b*]pyridazine nucleus by different 1,4-diaminocyclohexanes or cyclic amines was investigated. The dual kinase-RNase inhibition was maintained or enhanced by the additional presence of polar groups, but best aqueous solubility was obtained by integrating the ((*N*-methylpiperidin-4-yl)methyl) amine function. One of the most active compounds, **31,** exhibited nanomolar potency for biochemical inhibition of the kinase (IC_{50} = 160 nM) and RNase (IC_{50} = 80 nM) function. The high selectivity for IRE1 over other kinases was further improved (>70% inhibition of 4/455). It was speculated that this high kinome selectivity of **31** could be the result of the unusual IRE1 kinase binding mode displaying multiple structural disruptions. These findings further extend the knowledge on IRE1 kinase site binding modulators and help pave the way towards the discovery of new highly selective and cell-active inhibitors.

***Amino-Thienopyrimidines*: Compound 25**

From a high throughput screening of a 92K compounds library, Beveridge *et al.* recently identified compound **2**, an amino-quinazoline B-Raf kinase inhibitor (B-Raf K_i = 0.0023 μM), as a promising IRE1 inhibitor [55]. It demonstrated potent ATP-competitive IRE1 binding affinity (IRE1-TR-FRET IC_{50} = 0.0068 μM), but modest potency on IRE1 endoribonuclease activity in both an enzymatic RNase inhibition assay (IRE1-RNase IC_{50} = 0.200 μM) and a cellular X-box binding protein-1 splicing luciferase reporter assay (XBP1-luc IC_{50} = 5.58 μM). Obtention of a co-crystal structure of **2** bound to IRE1 (PDB

ID 6XDF) lifted the veil on the most predominant ligand interactions within the ATP pocket and some unique structural features of the complex (Figure 9A).

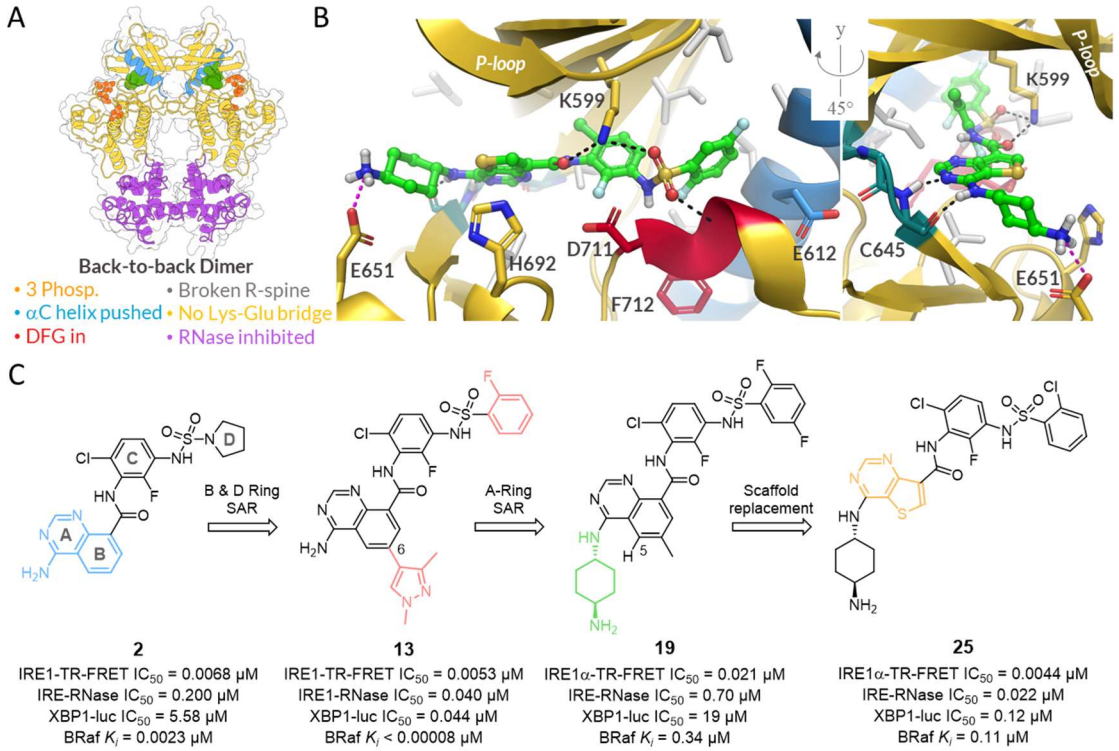

Figure 9. A. Graphical representation of the back-to-back dimer visible in the structure of *h*IRE1 in complex with compound 25 (PDB ID 6XDD). Key structural changes highlighted underneath. B. Front and left-side view of compound 25 in the kinase site. Key interactions and residues indicated. Color coding and representation as in Figure 2. C. Structural optimizations of compound 2 identified in a HTS campaign through SAR studies on ring A, B and D and finally scaffold replacement by a thienopyrimidine core, yielding compound 25. Structural changes highlighted in colors with bold bonds.

These crucial interactions include classical type I/II hinge contacts with the amino-quinazoline A-ring, strong hydrogen bonding from the sulfonamide to Asp711 and Phe712 of the DFG-motif, and occupation of the αC-helix pocket by pyrrolidine D-ring, thus breaking the Glu612-Lys599 bridge and pushing outward the αC-helix (Figure 9B). Other noteworthy features were the existence of a pseudoring by intramolecular hydrogen interaction between the amide group and one nitrogen of the quinazoline core, and, in contrast to the reference ligand **KIRA8**, no ionic interaction with Glu651. Guided by these observations, the authors conducted several SAR studies on targeted position of **2** aimed at improving potency for IRE1 while reducing B-Raf kinase binding affinity.

While searching for D-ring analogues within an in-house chemical library to explore their potential impact on αC-helix shift, the authors serendipitously discovered that a methyl substitution in position C-6 on the quinazoline B-ring improved cellular *XBP1* splicing inhibition by a ~10-fold factor. This result, combined with the close proximity of the imidazole ring of His692 (~ 4-5 Å from the quinazoline 6-position) in an unexplored polar pocket encouraged the authors to target this residue. Five and six-membered heterocycles (pyridines and pyrazoles) were thus introduced to interact *via* π–π stacking or hydrogen bonding. The novel analogues synthesized also incorporated chloro- or fluoro-phenyl sulfonamides D-rings, chosen to replace the original pyrrolidine. This first B-ring and D-ring SAR study led to compound **13** (Figure 9C), showing a 125-fold improvement in the XBP1 luciferase assay compared to the initial hit **2**, and for which a second crystal structure was solved (PDB ID 6XDB). In this structure, the 1,3-dimethyl-1*H*-pyrazol-4-yl group is engaged in a hydrogen bonding interaction with the imidazole of His692, as designed, and two weaker C-H hydrogen bonds between the two methyl groups and Leu577 and His579 are also observed. Unfortunately, these modifications also significantly increased the binding affinity towards the B-Raf kinase.

To overcome this, the non-conserved residue Glu651 in IRE1 (His539 in B-Raf) was targeted to gain in selectivity, a proven strategy for IRE1 inhibitors [64]. Some basic amino groups were selected for generating an ionic interaction with Glu651, while expected to clash with His539 in B-Raf. These novel modulations resulted in selection of the *trans*-diaminocyclohexane containing compound **19** (Figure 9C) which, although exhibiting reduced IRE1-TR-FRET binding potency (IC_{50} = 0.021 μM) and XBP1-luc inhibition (IC_{50} = 19 μM), also showed a strong drop in B-Raf binding potency (B-Raf K_i = 0.34 μM). Encouraged by these results and to explain the reduced activities observed, the authors turned their attention toward the effects of the *trans*-diaminocyclohexane on the ligand's predicted bioactive conformation interacting with the hinge backbone. Torsional analysis allowed them to identify a steric clash between the *trans*-diaminocyclohexane and aromatic C-H of the quinazoline ring system. The structurally related thienopyrimidine core - predicted to have a strongly reduced strain energy - was selected for further investigations. A set of amino substituted thienopyrimidines were synthesized and their activities were compared to their quinazoline analogues. This extensive SAR study allowed, at the end, to identify compound **25**, exhibiting good IRE1-XBP1 cellular potency and a ~50-fold decrease in B-Raf K_i potency, as a promising lead for further optimization. From this last series, the authors were able to obtain a crystal

structure of compound **23**, a close analogue of compound **25,** in complex with IRE1 (Figure 9B.) (PDB ID 6XDD) which allowed to confirm the establishment of a salt bridge between the *trans*-diaminocyclohexane and Glu651 as a strategy to improve IRE1 selectivity over B-Raf.

IRE1 RNase domain covalent ligands

Hydroxy aryl aldehydes: **MKC, OICR, 4μ8c, B-I09**

An alternative class of IRE1 modulators was identified during high-throughput screening attempts[70–72], that exhibit a different mode of action. This class of inhibitors shares a common hydroxy aryl aldehyde (HAA) moiety (Figure 10, A.) which was later demonstrated to covalently reacts with a specific nucleophile residue (Lys907) within the RNase domain of IRE1, resulting in the formation of a stable imine bond through a Schiff base reaction. The HAA modulators efficiently inhibit the RNase activity of IRE1 and thus prevent the ER stress-induced *XBP1* mRNA cleavage. Salicylaldehyde analogues were the first group of HAA inhibitors, discovered by Volkmann *et al*. in 2011 [70]. They found that salicylaldehyde analogues were active in inhibiting the site-specific cleavage of several mini-*XBP1* stem-loop RNAs in a dose-dependent manner. This class of compounds was also capable of blocking the transcriptional up-regulation of known XBP1 targets as well as mRNAs targeted for degradation by IRE1. Kinetic analysis showed that 3-ethoxy-5,6-dibromo-salicylaldehyde, a potent salicylaldehyde analog, acted as a non-competitive inhibitor to the *XBP1* mRNA substrate with an IC_{50} = 0.12 μM. Another salicylaldehyde analog, 3-methoxy-6-bromo-salicylaldehyde, heavily inhibited the *XBP1* splicing in an *in vivo* assay (IC_{50} = 0.41 μM) of acute ER stress. The salicylaldehyde analogues potent for *h*IRE1 were significantly less active for *y*IRE1 and inactive for murine IRE1. Different possibilities for the mode of action of the salicylaldehyde analogues were proposed, but it could not be determined with certainty whether the binding occurred near the RNase domain or at a new, distant, allosteric site.

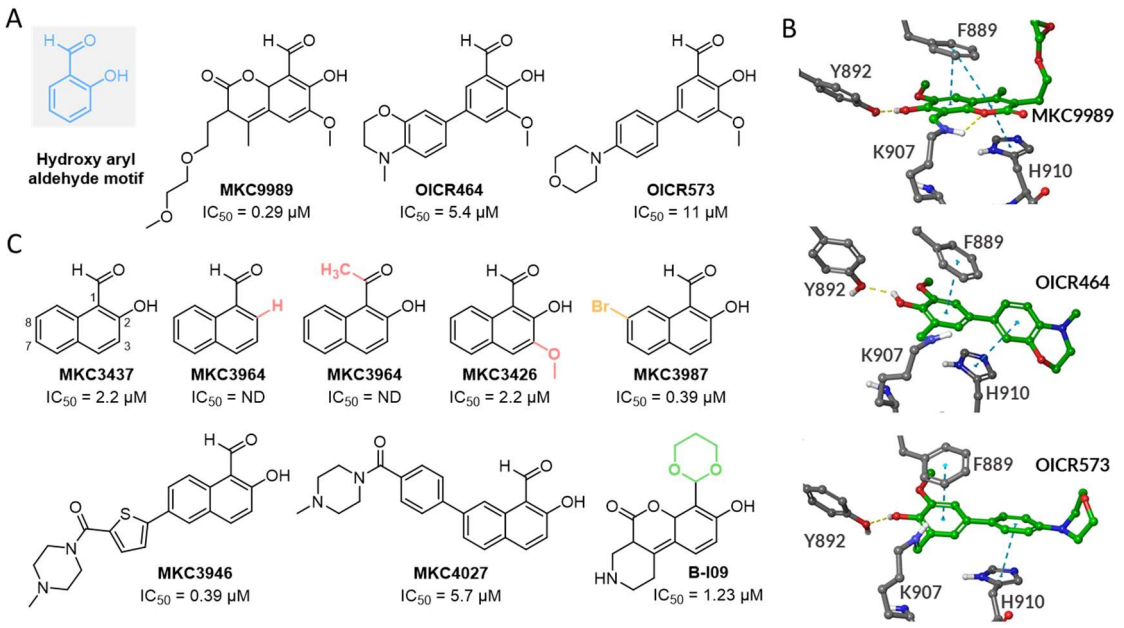

Figure 10. A. Molecular structures and B. binding modes of three HAA inhibitors (MKC9989, OICR464, and OICR573) identified and co-crystalized with murine IRE1 (PDB-IDs 4PL3, 4PL4, and 4PL5, respectively [3]. The blue and yellow dashed lines in panel B. represent π-π stacking and hydrogen bond interactions, respectively. C. SAR analysis using a series of HAA analogues around a naphthalene scaffold [7,8]. IC_{50} values are related to RNase inhibition of murine IRE1.

4-methyl umbelliferone 8-carbaldehyde (**4μ8C**) was the first dual-ring inhibitor in the HAA class, identified by Cross *et al.* [71] among a collection of 238,287 pure compounds. An *in vivo* IC_{50} = 4.6 μM was recorded for the compound in parallel concentration-response analyses of inhibition of XPB1 splicing. They proposed a covalent mode of action of 4μ8C by the fact that the inhibitor demonstrated non-competitive inhibition. Furthermore, the significance of the aldehyde moiety in the 4μ8C inhibitor was confirmed by the observation that the primary alcohol, the product of 4μ8C reduction by treatment with sodium borohydride, was completely inactive. Structural activity relationship analysis of 4μ8C indicated that substitution of the *ortho* hydroxyl in 4μ8C and related compounds abrogated the inhibition. By tracking the 4μ8C reactivity with IRE1, they could identify a highly selective residue, Lys907, in the RNase active site of which the aldehyde moiety reacts with the amine side chain and forms a stable Schiff base. Shortly after, Sanches *et al.* [72] solved three crystal structures (PDB IDs 4PL3, 4PL4 & 4PL5) of murine IRE1 in complex with three HAA inhibitors: **MKC9989**, **OICR573,** and **OICR464** (Figure 10A) that confirmed the binding site and Schiff base formation. These

HAA inhibitors potently inhibit the RNase activity of murine and *h*IRE1, and to a lesser degree *y*IRE1 *in vitro*, with IC_{50} values ranging from 0.23 to 44 μM, while they display no or only weak effect on the auto-phosphorylating activity of IRE1 even at the highest concentrations tested. They found that the potency of the three new HAA inhibitors significantly depended on the pre-incubation time with IRE1, which was interpreted as being linked to differences in reactivity of the aldehyde group in each HAA scaffold in the Schiff base formation with Lys907. In all three solved crystal structures, IRE1 was crystallized in the same face-to-face dimer form similar to *h*IRE1 [73], and not the back-to-back dimer [74] or oligomer configuration adopted by *y*IRE1[22]. **MKC9989**, **OICR573**, and **OICR464** all shared the same binding modes within a shallow hydrophobic pocket in the RNase domain, surrounded by helices α3′, α4, and α5 and residues Leu886, Phe889, Tyr892, Lys907, Glu913, Leu914, and Pro915 (Figure 10B): (1) a Schiff base interaction between the aldehyde moiety of the HAA and the amine side chain of Lys907; (2) a strong hydrogen bond interaction between the *ortho* hydroxy group of the HAAs and the side chain of Tyr892; (3) π-π stacking of the Phe889 side chain and the apical aromatic ring of the HAAs; and (4) π-π stacking of the His910 side chain and the basal aromatic ring of the HAAs. Mutational analysis revealed that any mutation placed on the residues Phe889, Tyr892, Asn906, His910, and Lys907 abolished the RNase activity of IRE1 against a single hairpin substrate. Structure activity relationship analysis was also performed using a series of HAA analogues around naphthalene and biphenyl scaffolds [75,76], which offers more substituent sites around the dual fused ring (Figure 10C) [32,77]. Consistent with the previous SAR analysis of single aryl ring HAA inhibitors [71], substitution of either aldehyde or *ortho* hydroxyl moieties, (position 1 and 2, respectively, Figure 10C) were not tolerated (**MKC3964** and **MKC3820**), reflecting the significance of the Schiff base interaction with Lys907 and the strong hydrogen bond with Tyr892. Substitution with bulky groups on positions 3 and 7, which are facing the solvent, were well tolerated (**MKC3426** and **MKC3946**). Bromine substitution at position 8 (**MKC3987**) was favored over hydrogen, while the bulkier group in **MKC4027** was predicted to cause steric clashes and thus considered as disfavored.

Tang *et al*. [78] introduced a novel set of HAA inhibitors with a tricyclic chromenone scaffold which were able to potently suppress the XBP1 expression and induce apoptosis. They also introduced a lead inhibitor, **B-I09** (IC_{50} = 1.23 μM), and determined its pharmacokinetics and bioavailability. In **B-I09**, the aldehyde group is protected using 1,3-dioxane as a putative prodrug moiety. Using LC-MS analysis they confirmed that the 1,3-

dioxane–protecting group remained after 2-days exposure to a FRET assay buffer and was 50% intact after 1-day incubation in cell culture medium, respectively. Based on these results and the bioactivity of **B-I09** compared to other derivatives, they elucidated that the 1,3-dioxane–protecting moiety enhances the cellular uptake and will be decomposed to expose the bioactive aldehyde group once inside the cell. Additional analogous HAA inhibitors sharing different scaffolds of naphthalene [75,76], single-ring and biphenyl [75], coumarin [79], and chromenone [80] were also identified and proved to be potent inhibitors of IRE1 RNase activity. The mystery behind the high selectivity of HAA inhibitors toward one of the specific Lysine residues (Lys907) among all 23 Lysine residues of IRE1 has been deciphered in two recent studies [81,82]. In a first study [82], the interaction of **MKC9989** molecules with two buried Lysine residues (Lys599 and Lys907) and two solvent-exposed ones (Lys656 and Lys799) as representative residues of IRE1 (PDB ID 4PL3), was investigated by means of molecular docking and extensive MD simulations. Based on the energetic diagrams and distance analysis of the MD trajectories, it was demonstrated that **MKC9989** is quite stable within the binding site of the two buried Lys907 and Lys599, while the interactions with the water-exposed ones are unfavorable. Since Lys599 is located within the kinase pocket, an endogenous ligand like ATP is expected to strongly compete with the inhibitors in binding to Lys599, which justifies their inactivity in IRE1 kinase inhibition. This was followed by a detailed exploration of the selectivity of the **MKC9989** inhibitor towards residue Lys907 using multiscale *in silico* techniques including Multi-Conformation Continuum Electrostatics (MCCE) simulations, Quantum Mechanics/Molecular Mechanics (QM/MM) calculations, covalent docking, and MD simulations [81]. According to these results, Lys907 is completely deprotonated within its hydrophobic pocket, which is an essential requirement for the initiation of the Schiff base reaction with the aldehyde moiety of the HAA molecules. QM/MM calculations and potential energy surface analysis revealed a spontaneous proton transfer (with ~0 energy barrier) from Lys907 to the adjacent Asp885, consistent with the low pK_a of Lys907 calculated using the MCCE method. Using covalent docking and MD simulations, it was verified that the hydrophobic pocket formed by Lys907 and its neighboring residues could effectively stabilize the **MKC9989** molecule by strong $\pi-\pi$ stacking and hydrogen bonding interactions. Furthermore, Radial Distribution Function (RDF) analysis confirmed that the imine bond formed during the Schiff base reaction between Lys907 and **MKC9989** is inaccessible for water molecules and thus the probability of imine hydrolysis is almost zero.

Concluding remarks

Here we discussed case by case the structural and molecular bases of reported IRE1 small-molecule modulators and detailed the discovery and structural development of their scaffolds. This overview highlights the significant advances made by the field in a relatively short time (~10 years) in the comprehension of IRE1 activation mechanism and pharmacological targeting of its catalytic sites. In particular, major milestones such as nanomolar potency, excellent kinase selectivity, and more recently exceptional control over the inter-dependent kinase-RNase relationship, have been achieved [54,55,59,64–66,68]. As indicated in the introduction and although not described within this manuscript for the sake of clarity and brevity, numerous new kinase-site binding inhibitors with novel scaffolds were patented since 2017 by pharmaceutical industrial groups & start-ups (Genentech and Paraza Pharma [83–86], Quentis therapeutics [87–94], OptiKIRA [95–99]). This recent increase in publications and patent applications testifies of the dynamism of the field and of the relevance of IRE1 as a therapeutic target. Hopefully, the recent rise in kinase inhibitors development described above will in the near future also translate into more compounds entering the clinics. As highlighted in this review, development of druglike small molecules targeting IRE1 activity has been mostly restricted to its catalytic sites. Nonetheless, a few other ligands and class of compounds have been reported to modulate IRE1 activity through different binding site and/or mode of action [49]. In particular, the naturally occurring flavonol quercetin [100] is worth mentioning as a crystal structure has been solved and showed the natural product to bind at the RNase domain interface of the IRE1 dimer. Targeting the RNase domain's dimer protein-protein interface has recently attracted interest has it has been shown that protomer alignment [101] and oligomerization state [102] can alter substrate specificity. Alternatively, we believe that IRE1 is an ideal candidate to explore a range of novel modalities that arose in medicinal chemistry. IRE1 is known to also exert scaffolding functions with partner proteins, which could be leveraged to reprogram its functions through the modulations of protein–protein interactions (PPIs) involving IRE1. The PPIs formed during the oligomerization process, or with partners such as BiP, HSP47, and the Sigma1 receptor, which fine-tune its activation level, Filamin A, RtcB or IP3 receptors, may represent appealing opportunities to develop PPI inhibitors or stabilizers [103–105]. Other trending modalities of interest are PROTACS (proteolysis targeting chimeras) and other chimeric degrader solutions [106–108]. These have already been applied with success to

826 transmembrane proteins with enzymatic activities similar to IRE1 [109] and the wide
827 range of high-affinity and selective IRE1 ligands available makes PROTACS a
828 compelling option to pursue. Finally, a fragment-based drug discovery (FBDD) program
829 applied to IRE1 could help finding molecular starting points that bind to non-catalytic
830 sites of the protein, which could be extremely valuable in the development of novel
831 allosteric inhibitors or PPI modulators [110–112].
832

833 **Abbreviations**

834 ATF6; activating transcription factor 6; BiP, bnding immunoglobulin protein; ER,
835 endoplasmic reticulum; HAAs, hydroxy-aryl aldehydes; HDX, hydrogen-deuterium
836 exchange; IPA, IRE1/PERK Activator; IRE1, inositol-requiring enzyme 1 alpha; PERK,
837 protein kinase R-like ER kinase; KIRAs, kinase inhibiting RNase attenuators; RIDD,
838 regulated IRE1α-dependent decay; SAR, structure-activity relationship; UPR, unfolded
839 protein response
840
841

ACKNOWLEDGEMENTS - This work was funded by grants from: Institut National du Cancer (INCa PLBIO), Fondation pour la Recherche Médicale (FRM, DEQ20180339169), ERANET and Agence Nationale de la Recherche (ERAAT) to EC; EU H2020 MSCA ITN-675448 (TRAINERS) and MSCA RISE-734749 (INSPIRED) grants to LAE, EC; Swedish Research Council (VR; grant number 2019-3684) grant to LAE; Vinnova Seal-of-Excellence program 2019-02205 (CaTheDRA) to SJM; TL thanks "Ecole Doctorale 3M" and university of Rennes 1 for his PhD research fellowship; DPR was funded by a grant from Région Bretagne and XG is grateful to the the Fondation ARC pour la recherche sur le cancer for his post-doctoral fellowship (PDF20191209830).

CONFLICT OF INTEREST - LEA and EC are founders of Cell Stress Discoveries Ltd. The authors declare no conflicting interests. EC is founder of Thabor Therapeutics.

ASSOCIATED CONTENTS - 2D molecular structures and SAR schemes have been drawn using ChemDraw Professional 20.0 (RRID:SCR_016768); Binding sites zoom-in pictures were generated using PyMOL 2.2.0 (RRID:SCR_000305); Graphical representation of IRE1 homo-multimers were generated using the Protein Imager online platform [113]; Crystallographic structures were retrieved from the RSCB wwPDB website (RRID:SCR_006555).

ORCID IDs:

D.P.R.: 0000-0002-9071-2380

N.G.: 0000-0002-5527-8566

F.C.: 0000-0002-7406-8353

S.J.M.: 0000-0002-4844-6234

E.C.: 0000-0001-5855-4522

L.A.E.: 0000-0001-5654-3109

X.G.: 0000-0001-5989-3833

References

1 Almanza, A., Carlesso, A., Chintha, C., Creedican, S., Doultsinos, D., Leuzzi, B., Luís, A., McCarthy, N., Montibeller, L., More, S., et al. (2019) Endoplasmic reticulum stress signalling – from basic mechanisms to clinical applications. The FEBS Journal **286**, 241–278.

2 Gagnon, E., Duclos, S., Rondeau, C., Chevet, E., Cameron, P. H., Steele-Mortimer, O., Paiement, J., Bergeron, J. J. M. and Desjardins, M. (2002) Endoplasmic Reticulum-Mediated Phagocytosis Is a Mechanism of Entry into Macrophages. Cell, Elsevier **110**, 119–131.

3 Bell, A. W., Ward, M. A., Blackstock, W. P., Freeman, H. N. M., Choudhary, J. S., Lewis, A. P., Chotai, D., Fazel, A., Gushue, J. N., Paiement, J., et al. (2001) Proteomics Characterization of Abundant Golgi Membrane Proteins *. Journal of Biological Chemistry, Elsevier **276**, 5152–5165.

4 Phillips, M. J. and Voeltz, G. K. (2016) Structure and function of ER membrane contact sites with other organelles. Nature Reviews Molecular Cell Biology, Nature Publishing Group **17**, 69–82.

5 Morel, E. (2020) Endoplasmic Reticulum Membrane and Contact Site Dynamics in Autophagy Regulation and Stress Response. Front Cell Dev Biol **8**, 343.

6 Hetz, C., Chevet, E. and Oakes, S. A. (2015) Proteostasis control by the unfolded protein response. Nat Cell Biol **17**, 829–838.

7 Iwawaki, T., Hosoda, A., Okuda, T., Kamigori, Y., Nomura-Furuwatari, C., Kimata, Y., Tsuru, A. and Kohno, K. (2001) Translational control by the ER transmembrane kinase/ribonuclease IRE1 under ER stress. Nat Cell Biol **3**, 158–164.

8 Grey, M. J., Cloots, E., Simpson, M. S., LeDuc, N., Serebrenik, Y. V., De Luca, H., De Sutter, D., Luong, P., Thiagarajah, J. R., Paton, A. W., et al. (2020) IRE1β negatively regulates IRE1α signaling in response to endoplasmic reticulum stress. Journal of Cell Biology **219**.

9 Kimata, Y., Oikawa, D., Shimizu, Y., Ishiwata-Kimata, Y. and Kohno, K. (2004) A role for BiP as an adjustor for the endoplasmic reticulum stress-sensing protein Ire1. J Cell Biol **167**, 445–456.

10 Pincus, D., Chevalier, M. W., Aragón, T., van Anken, E., Vidal, S. E., El-Samad, H. and Walter, P. (2010) BiP binding to the ER-stress sensor Ire1 tunes the homeostatic behavior of the unfolded protein response. PLoS Biol **8**, e1000415.

11 Lu, Y., Liang, F.-X. and Wang, X. (2014) A Synthetic Biology Approach Identifies the Mammalian UPR RNA Ligase RtcB. Molecular Cell, Elsevier **55**, 758–770.

12 Kosmaczewski, S. G., Edwards, T. J., Han, S. M., Eckwahl, M. J., Meyer, B. I., Peach, S., Hesselberth, J. R., Wolin, S. L. and Hammarlund, M. (2014) The RtcB RNA ligase is an essential component of the metazoan unfolded protein response. EMBO Rep **15**, 1278–1285.

13 Jurkin, J., Henkel, T., Nielsen, A. F., Minnich, M., Popow, J., Kaufmann, T., Heindl, K., Hoffmann, T., Busslinger, M. and Martinez, J. (2014) The mammalian tRNA ligase complex mediates splicing of XBP1 mRNA and controls antibody secretion in plasma cells. EMBO J **33**, 2922–2936.

14 Hollien, J. and Weissman, J. S. (2006) Decay of Endoplasmic Reticulum-Localized mRNAs During the Unfolded Protein Response. Science, American Association for the Advancement of Science **313**, 104–107.

15 Maurel, M., Chevet, E., Tavernier, J. and Gerlo, S. (2014) Getting RIDD of RNA: IRE1 in cell fate regulation. Trends in Biochemical Sciences **39**, 245–254.

16 Upton, J.-P., Wang, L., Han, D., Wang, E. S., Huskey, N. E., Lim, L., Truitt, M., McManus, M. T., Ruggero, D., Goga, A., et al. (2012) IRE1α Cleaves Select microRNAs During ER Stress to Derepress Translation of Proapoptotic Caspase-2. Science, American Association for the Advancement of Science **338**, 818–822.

17 Lhomond, S., Avril, T., Dejeans, N., Voutetakis, K., Doultsinos, D., McMahon, M., Pineau, R., Obacz, J., Papadodima, O., Jouan, F., et al. (2018) Dual IRE1 RNase functions dictate glioblastoma development. EMBO Molecular Medicine **10**, e7929.

18 Hetz, C. and Glimcher, L. H. (2009) Fine-tuning of the unfolded protein response: Assembling the IRE1alpha interactome. Mol Cell **35**, 551–561.

19 Sepulveda, D., Rojas-Rivera, D., Rodríguez, D. A., Groenendyk, J., Köhler, A., Lebeaupin, C., Ito, S., Urra, H., Carreras-Sureda, A., Hazari, Y., et al. (2018) Interactome Screening Identifies the ER Luminal Chaperone Hsp47 as a Regulator of the Unfolded Protein Response Transducer IRE1α. Molecular Cell **69**, 238-252.e7.

20 Yan, C., Liu, J., Gao, J., Sun, Y., Zhang, L., Song, H., Xue, L., Zhan, L., Gao, G., Ke, Z., et al. (2019) IRE1 promotes neurodegeneration through autophagy-dependent neuron death in the Drosophila model of Parkinson's disease. Cell Death & Disease, Nature Publishing Group **10**, 1–15.

937 21 Duran-Aniotz, C., Cornejo, V. H., Espinoza, S., Ardiles, Á. O., Medinas, D. B.,
938 Salazar, C., Foley, A., Gajardo, I., Thielen, P., Iwawaki, T., et al. (2017) IRE1
939 signaling exacerbates Alzheimer's disease pathogenesis. Acta Neuropathol **134**,
940 489–506.
941 22 Korennykh, A. V., Egea, P. F., Korostelev, A. A., Finer-Moore, J., Zhang, C.,
942 Shokat, K. M., Stroud, R. M. and Walter, P. (2009) The unfolded protein response
943 signals through high-order assembly of Ire1. Nature, Nature Publishing Group **457**,
944 687–693.
945 23 Kiskinis, E., Sandoe, J., Williams, L. A., Boulting, G. L., Moccia, R., Wainger, B.
946 J., Han, S., Peng, T., Thams, S., Mikkilineni, S., et al. (2014) Pathways disrupted in
947 human ALS motor neurons identified through genetic correction of mutant SOD1.
948 Cell Stem Cell **14**, 781–795.
949 24 Korovesis, D., Rufo, N., Derua, R., Agostinis, P. and Verhelst, S. H. L. (2020)
950 Kinase Photoaffinity Labeling Reveals Low Selectivity Profile of the IRE1
951 Targeting Imidazopyrazine-Based KIRA6 Inhibitor. ACS Chem. Biol. **15**, 3106–
952 3111.
953 25 Palumbo, A., Gay, F., Bringhen, S., Falcone, A., Pescosta, N., Callea, V., Caravita,
954 T., Morabito, F., Magarotto, V., Ruggeri, M., et al. (2008) Bortezomib, doxorubicin
955 and dexamethasone in advanced multiple myeloma. Annals of Oncology **19**, 1160–
956 1165.
957 26 Wang, J.-M., Qiu, Y., Yang, Z., Kim, H., Qian, Q., Sun, Q., Zhang, C., Yin, L.,
958 Fang, D., Back, S. H., et al. (2018) IRE1α prevents hepatic steatosis by processing
959 and promoting the degradation of select microRNAs. Sci. Signal., American
960 Association for the Advancement of Science **11**.
961 27 Lipson, K. L., Fonseca, S. G., Ishigaki, S., Nguyen, L. X., Foss, E., Bortell, R.,
962 Rossini, A. A. and Urano, F. (2006) Regulation of insulin biosynthesis in pancreatic
963 beta cells by an endoplasmic reticulum-resident protein kinase IRE1. Cell Metab **4**,
964 245–254.
965 28 Lee, H., Lee, Y.-S., Harenda, Q., Pietrzak, S., Oktay, H. Z., Schreiber, S., Liao, Y.,
966 Sonthalia, S., Ciecko, A. E., Chen, Y.-G., et al. (2020) Beta Cell Dedifferentiation
967 Induced by IRE1α Deletion Prevents Type 1 Diabetes. Cell Metab **31**, 822-836.e5.
968 29 Kaser, A. and Blumberg, R. S. (2009) Endoplasmic reticulum stress in the intestinal
969 epithelium and inflammatory bowel disease. Seminars in Immunology **21**, 156–163.

30 Tschurtschenthaler, M., Adolph, T. E., Ashcroft, J. W., Niederreiter, L., Bharti, R., Saveljeva, S., Bhattacharyya, J., Flak, M. B., Shih, D. Q., Fuhler, G. M., et al. (2017) Defective ATG16L1-mediated removal of IRE1α drives Crohn's disease-like ileitis. J Exp Med **214**, 401–422.

31 Harnoss, J. M., Thomas, A. L., Shemorry, A., Marsters, S. A., Lawrence, D. A., Lu, M., Chen, Y.-C. A., Qing, J., Totpal, K., Kan, D., et al. (2019) Disruption of IRE1α through its kinase domain attenuates multiple myeloma. PNAS, National Academy of Sciences **116**, 16420–16429.

32 Mimura, N., Fulciniti, M., Gorgun, G., Tai, Y.-T., Cirstea, D., Santo, L., Hu, Y., Fabre, C., Minami, J., Ohguchi, H., et al. (2012) Blockade of XBP1 splicing by inhibition of IRE1α is a promising therapeutic option in multiple myeloma. Blood **119**, 5772–5781.

33 Sun, H., Lin, D.-C., Guo, X., Kharabi Masouleh, B., Gery, S., Cao, Q., Alkan, S., Ikezoe, T., Akiba, C., Paquette, R., et al. (2016) Inhibition of IRE1α-driven pro-survival pathways is a promising therapeutic application in acute myeloid leukemia. Oncotarget **7**, 18736–18749.

34 Sheng, X., Nenseth, H. Z., Qu, S., Kuzu, O. F., Frahnow, T., Simon, L., Greene, S., Zeng, Q., Fazli, L., Rennie, P. S., et al. (2019) IRE1α-XBP1s pathway promotes prostate cancer by activating c-MYC signaling. Nature Communications, Nature Publishing Group **10**, 323.

35 Song, M., Sandoval, T. A., Chae, C.-S., Chopra, S., Tan, C., Rutkowski, M. R., Raundhal, M., Chaurio, R. A., Payne, K. K., Konrad, C., et al. (2018) IRE1α–XBP1 controls T cell function in ovarian cancer by regulating mitochondrial activity. Nature, Nature Publishing Group **562**, 423–428.

36 Harnoss, J. M., Le Thomas, A., Reichelt, M., Guttman, O., Wu, T. D., Marsters, S. A., Shemorry, A., Lawrence, D. A., Kan, D., Segal, E., et al. (2020) IRE1α Disruption in Triple-Negative Breast Cancer Cooperates with Antiangiogenic Therapy by Reversing ER Stress Adaptation and Remodeling the Tumor Microenvironment. Cancer Res **80**, 2368–2379.

37 Logue, S. E., McGrath, E. P., Cleary, P., Greene, S., Mnich, K., Almanza, A., Chevet, E., Dwyer, R. M., Oommen, A., Legembre, P., et al. (2018) Inhibition of IRE1 RNase activity modulates the tumor cell secretome and enhances response to chemotherapy. Nat Commun **9**, 3267.

38 Gu, Q., Zhu, C., Wu, X., Peng, L., Huang, G. and Hu, R. (2021) Wogonoside promotes apoptosis and ER stress in human gastric cancer cells by regulating the IRE1α pathway. Exp Ther Med **21**, 411.

39 Kim, J. L., Lee, D.-H., Jeong, S., Kim, B. R., Na, Y. J., Park, S. H., Jo, M. J., Jeong, Y. A. and Oh, S. C. (2019) Imatinib-induced apoptosis of gastric cancer cells is mediated by endoplasmic reticulum stress. Oncol Rep **41**, 1616–1626.

40 Kim, T. W., Lee, S. Y., Kim, M., Cheon, C. and Ko, S.-G. (2018) Kaempferol induces autophagic cell death via IRE1-JNK-CHOP pathway and inhibition of G9a in gastric cancer cells. Cell Death & Disease, Nature Publishing Group **9**, 1–14.

41 Pavlović, N., Calitz, C., Thanapirom, K., Mazza, G., Rombouts, K., Gerwins, P. and Heindryckx, F. (2020) Inhibiting IRE1α-endonuclease activity decreases tumor burden in a mouse model for hepatocellular carcinoma. eLife (Postovit, L.-M., Ojala, P. M., and Postovit, L.-M., eds.), eLife Sciences Publications, Ltd **9**, e55865.

42 Liu, D., Liu, X., Zhou, T., Yao, W., Zhao, J., Zheng, Z., Jiang, W., Wang, F., Aikhionbare, F. O., Hill, D. L., et al. (2016) IRE1-RACK1 axis orchestrates ER stress preconditioning-elicited cytoprotection from ischemia/reperfusion injury in liver. J Mol Cell Biol **8**, 144–156.

43 Le Reste, P. J., Pineau, R., Voutetakis, K., Samal, J., Jégou, G., Lhomond, S., Gorman, A. M., Samali, A., Patterson, J. B., Zeng, Q., et al. (2020) Local intracerebral inhibition of IRE1 by MKC8866 sensitizes glioblastoma to irradiation/chemotherapy in vivo. Cancer Letters **494**, 73–83.

44 Doultsinos, D., Carlesso, A., Chintha, C., Paton, J. C., Paton, A. W., Samali, A., Chevet, E. and Eriksson, L. A. (2021) Peptidomimetic-based identification of FDA-approved compounds inhibiting IRE1 activity. The FEBS Journal **288**, 945–960.

45 Hetz, C., Axten, J. M. and Patterson, J. B. (2019) Pharmacological targeting of the unfolded protein response for disease intervention. Nature Chemical Biology, Nature Publishing Group **15**, 764–775.

46 Roskoski, R. (2016) Classification of small molecule protein kinase inhibitors based upon the structures of their drug-enzyme complexes. Pharmacological Research **103**, 26–48.

47 Martinez, R., Defnet, A. and Shapiro, P. (2020) Avoiding or Co-Opting ATP Inhibition: Overview of Type III, IV, V, and VI Kinase Inhibitors. In Next Generation Kinase Inhibitors: Moving Beyond the ATP Binding/Catalytic Sites (Shapiro, P., ed.), pp 29–59, Springer International Publishing, Cham.

48 Gehringer, M. and Laufer, S. A. (2019) Emerging and Re-Emerging Warheads for Targeted Covalent Inhibitors: Applications in Medicinal Chemistry and Chemical Biology. J. Med. Chem., American Chemical Society **62**, 5673–5724.

49 Raymundo, D. P., Doultsinos, D., Guillory, X., Carlesso, A., Eriksson, L. A. and Chevet, E. (2020) Pharmacological Targeting of IRE1 in Cancer. Trends in Cancer.

50 Korennykh, A. and Walter, P. (2012) Structural Basis of the Unfolded Protein Response. Annual Review of Cell and Developmental Biology **28**, 251–277.

51 Mendez, A. S., Alfaro, J., Morales-Soto, M. A., Dar, A. C., McCullagh, E., Gotthardt, K., Li, H., Acosta-Alvear, D., Sidrauski, C., Korennykh, A. V., et al. (2015) Endoplasmic reticulum stress-independent activation of unfolded protein response kinases by a small molecule ATP-mimic. eLife (Kuriyan, J., ed.), eLife Sciences Publications, Ltd **4**, e05434.

52 Potashman, M. H., Bready, J., Coxon, A., DeMelfi, Thomas M., DiPietro, L., Doerr, N., Elbaum, D., Estrada, J., Gallant, P., Germain, J., et al. (2007) Design, Synthesis, and Evaluation of Orally Active Benzimidazoles and Benzoxazoles as Vascular Endothelial Growth Factor-2 Receptor Tyrosine Kinase Inhibitors. J. Med. Chem., American Chemical Society **50**, 4351–4373.

53 Newbatt, Y., Hardcastle, A., McAndrew, P. C., Strover, J. A., Mirza, A., Morgan, G. J., Burke, R., Davies, F. E., Collins, I. and van Montfort, R. L. M. (2013) Identification of Autophosphorylation Inhibitors of the Inositol-Requiring Enzyme 1 Alpha (IRE1α) by High-Throughput Screening Using a DELFIA Assay. J Biomol Screen, SAGE Publications Inc STM **18**, 298–308.

54 Ferri, E., Le Thomas, A., Wallweber, H. A., Day, E. S., Walters, B. T., Kaufman, S. E., Braun, M.-G., Clark, K. R., Beresini, M. H., Mortara, K., et al. (2020) Activation of the IRE1 RNase through remodeling of the kinase front pocket by ATP-competitive ligands. Nature Communications, Nature Publishing Group **11**, 6387.

55 Beveridge, R. E., Wallweber, H. A., Ashkenazi, A., Beresini, M., Clark, K. R., Gibbons, P., Ghiro, E., Kaufman, S., Larivée, A., Leblanc, M., et al. (2020) Identification of BRaf-Sparing Amino-Thienopyrimidines with Potent IRE1α Inhibitory Activity. ACS Med. Chem. Lett., American Chemical Society.

56 Joshi, A., Newbatt, Y., McAndrew, P. C., Stubbs, M., Burke, R., Richards, M. W., Bhatia, C., Caldwell, J. J., McHardy, T., Collins, I., et al. (2015) Molecular mechanisms of human IRE1 activation through dimerization and ligand binding. Oncotarget **6**, 13019–13035.

57 Liu, Y. and Gray, N. S. (2006) Rational design of inhibitors that bind to inactive kinase conformations. Nature Chemical Biology, Nature Publishing Group **2**, 358–364.

58 Dar, A. C., Lopez, M. S. and Shokat, K. M. (2008) Small Molecule Recognition of c-Src via the Imatinib-Binding Conformation. Chem Biol **15**, 1015–1022.

59 Feldman, H. C., Tong, M., Wang, L., Meza-Acevedo, R., Gobillot, T. A., Lebedev, I., Gliedt, M. J., Hari, S. B., Mitra, A. K., Backes, B. J., et al. (2016) Structural and Functional Analysis of the Allosteric Inhibition of IRE1α with ATP-Competitive Ligands. ACS Chem. Biol. **11**, 2195–2205.

60 Catalano, A., Iacopetta, D., Sinicropi, M. S. and Franchini, C. (2021) Diarylureas as Antitumor Agents. Applied Sciences, Multidisciplinary Digital Publishing Institute **11**, 374.

61 Zhao, Z., Wu, H., Wang, L., Liu, Y., Knapp, S., Liu, Q. and Gray, N. S. (2014) Exploration of Type II Binding Mode: A Privileged Approach for Kinase Inhibitor Focused Drug Discovery? ACS Chem. Biol., American Chemical Society **9**, 1230–1241.

62 Ghosh, R., Wang, L., Wang, E. S., Perera, B. G. K., Igbaria, A., Morita, S., Prado, K., Thamsen, M., Caswell, D., Macias, H., et al. (2014) Allosteric Inhibition of the IRE1α RNase Preserves Cell Viability and Function during Endoplasmic Reticulum Stress. Cell **158**, 534–548.

63 Thamsen, M., Ghosh, R., Auyeung, V. C., Brumwell, A., Chapman, H. A., Backes, B. J., Perara, G., Maly, D. J., Sheppard, D. and Papa, F. R. (2019) Small molecule inhibition of IRE1α kinase/RNase has anti-fibrotic effects in the lung. PLoS ONE (Koval, M., ed.) **14**, e0209824.

64 Harrington, P. E., Biswas, K., Malwitz, D., Tasker, A. S., Mohr, C., Andrews, K. L., Dellamaggiore, K., Kendall, R., Beckmann, H., Jaeckel, P., et al. (2015) Unfolded Protein Response in Cancer: IRE1α Inhibition by Selective Kinase Ligands Does Not Impair Tumor Cell Viability. ACS Med. Chem. Lett. **6**, 68–72.

65 Feldman, H. C., Vidadala, V. N., Potter, Z. E., Papa, F. R., Backes, B. J. and Maly, D. J. (2019) Development of a Chemical Toolset for Studying the Paralog-Specific Function of IRE1. ACS Chem. Biol., American Chemical Society **14**, 2595–2605.

66 Concha, N. O., Smallwood, A., Bonnette, W., Totoritis, R., Zhang, G., Federowicz, K., Yang, J., Qi, H., Chen, S., Campobasso, N., et al. (2015) Long-Range Inhibitor-

Induced Conformational Regulation of Human IRE1α Endoribonuclease Activity. Mol Pharmacol **88**, 1011–1023.

67 Palmieri, L. and Rastelli, G. (2013) αC helix displacement as a general approach for allosteric modulation of protein kinases. Drug Discovery Today **18**, 407–414.

68 Colombano, G., Caldwell, J. J., Matthews, T. P., Bhatia, C., Joshi, A., McHardy, T., Mok, N. Y., Newbatt, Y., Pickard, L., Strover, J., et al. (2019) Binding to an Unusual Inactive Kinase Conformation by Highly Selective Inhibitors of Inositol-Requiring Enzyme 1α Kinase-Endoribonuclease. J. Med. Chem. **62**, 2447–2465.

69 Armstrong, M. C., Šestak, S., Ali, A. A., Sagini, H. A. M., Brown, M., Baty, K., Treumann, A. and Schröder, M. (2017) Bypass of Activation Loop Phosphorylation by Aspartate 836 in Activation of the Endoribonuclease Activity of Ire1. Molecular and Cellular Biology, American Society for Microbiology Journals **37**.

70 Volkmann, K., Lucas, J. L., Vuga, D., Wang, X., Brumm, D., Stiles, C., Kriebel, D., Der-Sarkissian, A., Krishnan, K., Schweitzer, C., et al. (2011) Potent and selective inhibitors of the inositol-requiring enzyme 1 endoribonuclease. J. Biol. Chem. **286**, 12743–12755.

71 Cross, B. C. S., Bond, P. J., Sadowski, P. G., Jha, B. K., Zak, J., Goodman, J. M., Silverman, R. H., Neubert, T. A., Baxendale, I. R., Ron, D., et al. (2012) The molecular basis for selective inhibition of unconventional mRNA splicing by an IRE1-binding small molecule. Proc Natl Acad Sci U S A **109**, E869–E878.

72 Sanches, M., Duffy, N. M., Talukdar, M., Thevakumaran, N., Chiovitti, D., Canny, M. D., Lee, K., Kurinov, I., Uehling, D., Al-awar, R., et al. (2014) Structure and mechanism of action of the hydroxy–aryl–aldehyde class of IRE1 endoribonuclease inhibitors. Nature Communications **5**, 4202.

73 Ali, M. M. U., Bagratuni, T., Davenport, E. L., Nowak, P. R., Silva-Santisteban, M. C., Hardcastle, A., McAndrews, C., Rowlands, M. G., Morgan, G. J., Aherne, W., et al. (2011) Structure of the Ire1 autophosphorylation complex and implications for the unfolded protein response. The EMBO Journal, John Wiley & Sons, Ltd **30**, 894–905.

74 Lee, K. P. K., Dey, M., Neculai, D., Cao, C., Dever, T. E. and Sicheri, F. (2008) Structure of the Dual Enzyme Ire1 Reveals the Basis for Catalysis and Regulation in Nonconventional RNA Splicing. Cell **132**, 89–100.

75 Patterson, J. B. and Lonergan, D. G. (2008, December 18) Ire-1a Inhibitors.

76 Zeng, Q., Wade, W. S. and Patterson, J. B. (2011, May 12) IRE-1 a INHIBITORS.

77 Mahoney, D. J., Lefebvre, C., Allan, K., Brun, J., Sanaei, C. A., Baird, S., Pearce, N., Grönberg, S., Wilson, B., Prakesh, M., et al. (2011) Virus-Tumor Interactome Screen Reveals ER Stress Response Can Reprogram Resistant Cancers for Oncolytic Virus-Triggered Caspase-2 Cell Death. Cancer Cell, Elsevier **20**, 443–456.

78 Tang, C.-H. A., Ranatunga, S., Kriss, C. L., Cubitt, C. L., Tao, J., Pinilla-Ibarz, J. A., Valle, J. R. D. and Hu, C.-C. A. (2014) Inhibition of ER stress–associated IRE-1/XBP-1 pathway reduces leukemic cell survival. J Clin Invest, American Society for Clinical Investigation **124**, 2585–2598.

79 Zeng, Q., Toro, A., Patterson, J. B., Wade, W. S., Zubovics, Z., Yang, Y. and Wu, Z. (2011, October 13) IRE-1a INHIBITORS.

80 Hu, C.-C. and Del, V. J. R. (2019, October 10) Substituted Chromenones, Ire1 Inhibitors, and Methods of Using Same.

81 Mahdizadeh, S. J., Carlesso, A. and Eriksson, L. A. (2020) Deciphering the selectivity of inhibitor MKC9989 towards residue K907 in IRE1α; a multiscale in silico approach. RSC Adv., The Royal Society of Chemistry **10**, 19720–19729.

82 Carlesso, A. and Eriksson, L. A. (2019) Selective Inhibition of IRE1 Signalling mediated by MKC9989: New Insights from Molecular Docking and Molecular Dynamics Simulations. ChemistrySelect **4**, 3199–3203.

83 Braun, M.-G., Castanedo, G., Gibbons, P., Rudolph, J., Vernier, W., Beveridge, R., Wu, Y. and Wu, G. (2020, July 9) Pyrido-Pyrimidinone and Pteridinone Compounds as Inhibitors of Endoribonuclease Inositol Requiring Enzyme I (ire I Alpha) for the Treatment of Cancer Diseases.

84 Braun, M.-G., Gibbons, P., Lee, W., Ly, C., Rudolph, J., Schwarz, J., Ashkenazi, A., Fu, L., Lai, T., Wang, F., et al. (2018, September 20) Pyrimidinyl-Pyridyloxy-Naphthyl Compounds and Methods of Treating Ire1-Related Diseases and Disorders.

85 Braun, M.-G., Ly, C. Q., Castanedo, G., Gibbons, P., Lee, W., Rudolph, J., Blaquiere, N. A., Schwarz, J. B., Beveridge, R., Leclerc, J.-P., et al. (2020, March 19) Phenoxy-Pyridyl-Pyrimidine Compounds and Methods of Use.

86 Braun, M.-G., Gibbons, P., Lee, W., Ly, C. Q., Rudolph, J., Schwarz, J. B., Ashkenazi, A., Beveridge, R., Zhao, L., Lemire, A., et al. (2020, March 19) Pyrimidinyl-Heteroaryloxy-Naphthyl Compounds and Methods of Use.

87 Glimcher, L. H., Bettigole, S. E., Ruiz, J. R. C. and Vacca, J. P. (2017, September 8) Small Molecule Ire1-Alpha Inhibitors.
88 Vacca, J. P., Li, D. and Bettigole, S. (2018, December 6) Ire1 Small Molecule Inhibitors.
89 Vacca, J. P., Li, D. and Bettigole, S. (2018, June 7) Ire1 Small Molecule Inhibitors.
90 Glimcher, L. H., Cubillos-Ruiz, J. R., Bettigole, S. E. and Vacca, J. P. (2018, September 7) Small Molecule Ire1-Alpha Inhibitors.
91 Vacca, J. P., Li, D. and Bettigole, S. E. (2020, November 19) Combination Therapies with Ire1 Small Molecule Inhibitors.
92 Vacca, J. P., Li, D. and Bettigole, S. E. (2020, November 19) Treatment of Fibrosis with Ire1 Small Molecule Inhibitors.
93 Vacca, J. P. and Bettigole, S. (2020, June 11) Ire1 Small Molecule Inhibitors.
94 Vacca, J. P. and Bettigole, S. (2020, June 11) Ire1 Small Molecule Inhibitors.
95 Keenan, R., Sutton, J. and Hynd, G. (2020, September 3) Pyrazolopyridine Compounds for Ire1 Inhibition.
96 Keenan, R., Sutton, J. and Hynd, G. (2020, September 3) Imidazolopyrazine Compounds for Ire1 Inhibition.
97 Backes, B., Papa, F., Oakes, S. and Maly, D. (2020, March 5) Ire1 Kinase Inhibitors and Uses Thereof.
98 Keenan, R. M., Backes, B. J., Maly, D. J., Reynolds, C., Whittaker, B., Knight, J., Sutton, J., Hynd, G., Papa, F. and Oakes, S. (2019, March 7) Compounds and Compositions for Ire1 Inhibition.
99 Backes, B. J., Maly, D. J., Oakes, S. a, Papa, F. R., Perera, G. and Wang, L. (2014, April 3) Modulation of Ire1.
100 Wiseman, R. L., Zhang, Y., Lee, K. P. K., Harding, H. P., Haynes, C. M., Price, J., Sicheri, F. and Ron, D. (2010) Flavonol activation defines an unanticipated ligand-binding site in the kinase-RNase domain of IRE1. Mol Cell **38**, 291–304.
101 Li, W., Crotty, K., Garrido Ruiz, D., Voorhies, M., Rivera, C., Sil, A., Mullins, R. D., Jacobson, M. P., Peschek, J. and Walter, P. (2021) Protomer alignment modulates specificity of RNA substrate recognition by Ire1. eLife (Sonenberg, N., Malhotra, V., and Korennykh, A. V., eds.), eLife Sciences Publications, Ltd **10**, e67425.
102 Thomas, A. L., Ferri, E., Marsters, S., Harnoss, J. M., Modrusan, Z., Li, W., Rudolph, J., Wang, W., Wu, T. D., Walter, P., et al. (2021) Noncanonical mRNA

1205 decay by the endoplasmic-reticulum stress sensor IRE1α promotes cancer-cell
1206 survival. bioRxiv, Cold Spring Harbor Laboratory 2021.03.16.435520.
1207 103 Korennykh, A. V., Egea, P. F., Korostelev, A. A., Finer-Moore, J., Stroud, R. M.,
1208 Zhang, C., Shokat, K. M. and Walter, P. (2011) Cofactor-mediated conformational
1209 control in the bifunctional kinase/RNase Ire1. BMC Biology, BioMed Central **9**, 48.
1210 104 Scott, D. E., Bayly, A. R., Abell, C. and Skidmore, J. (2016, July 29) Small
1211 molecules, big targets: Drug discovery faces the protein-protein interaction
1212 challenge. Nature Reviews Drug Discovery, Nature Publishing Group.
1213 105 Arkin, M. R., Tang, Y. and Wells, J. A. (2014, September 18) Small-molecule
1214 inhibitors of protein-protein interactions: Progressing toward the reality. Chemistry
1215 and Biology, Elsevier Ltd.
1216 106 Churcher, I. (2018) Protac-Induced Protein Degradation in Drug Discovery:
1217 Breaking the Rules or Just Making New Ones? Journal of Medicinal Chemistry,
1218 American Chemical Society **61**, 444–452.
1219 107 Wu, T., Yoon, H., Xiong, Y., Dixon-Clarke, S. E., Nowak, R. P. and Fischer, E. S.
1220 (2020) Targeted protein degradation as a powerful research tool in basic biology and
1221 drug target discovery. Nature Structural & Molecular Biology, Nature Publishing
1222 Group 1–10.
1223 108 Nalawansha, D. A. and Crews, C. M. (2020) PROTACs: An Emerging Therapeutic
1224 Modality in Precision Medicine. Cell Chemical Biology.
1225 109 Bondeson, D. P., Mares, A., Smith, I. E. D., Ko, E., Campos, S., Miah, A. H.,
1226 Mulholland, K. E., Routly, N., Buckley, D. L., Gustafson, J. L., et al. (2015)
1227 Catalytic in vivo protein knockdown by small-molecule PROTACs. Nature
1228 Chemical Biology, Nature Publishing Group **11**, 611–617.
1229 110 Erlanson, D. A., Fesik, S. W., Hubbard, R. E., Jahnke, W. and Jhoti, H. (2016,
1230 August 30) Twenty years on: The impact of fragments on drug discovery. Nature
1231 Reviews Drug Discovery, Nature Publishing Group.
1232 111 Erlanson, D. A., de Esch, I. J. P., Jahnke, W., Johnson, C. N. and Mortenson, P. N.
1233 (2020) Fragment-to-Lead Medicinal Chemistry Publications in 2018. Journal of
1234 Medicinal Chemistry, American Chemical Society (ACS).
1235 112 Guillory, X., Wolter, M., Leysen, S., Neves, J. F., Kuusk, A., Genet, S., Somsen, B.,
1236 Morrow, J. K., Rivers, E., van Beek, L., et al. (2020) Fragment-based Differential
1237 Targeting of PPI Stabilizer Interfaces. J. Med. Chem., American Chemical Society
1238 **63**, 6694–6707.

113 Tomasello, G., Armenia, I. and Molla, G. (2020) The Protein Imager: a full-featured online molecular viewer interface with server-side HQ-rendering capabilities. Bioinformatics **36**, 2909–2911.